Astron. Astrophys. 328, 649–669 (1997)

ASTRONOMY AND ASTROPHYSICS

Infrared spectroscopy of interstellar apolar ice analogs

P. Ehrenfreund[1], **A.C.A. Boogert**[2], **P.A. Gerakines**[1,3], **A.G.G.M. Tielens**[4], **and E.F. van Dishoeck**[1]

[1] Leiden Observatory, P.O. Box 9513, 2300 RA Leiden, The Netherlands
[2] Kapteyn Astronomical Institute, P.O. Box 800, 9700 AV Groningen, The Netherlands
[3] Department of Physics, Applied Physics & Astronomy, Rensselaer Polytechnic Institute, Troy, NY 12180-3590, USA
[4] NASA Ames Research Center, Mail Stop 245-6, Moffett Field, CA 94035, USA

Received 23 April 1997 / Accepted 22 July 1997

Abstract. Apolar ices have been observed in several regions in dense clouds and are likely dominated by molecules such as CO, CO_2 and the infrared inactive molecules O_2 and N_2. Interstellar solid CO has been well characterized by ground-based high resolution measurements. Recent ISO results showed the ubiquitous presence of abundant CO_2 ice and the presence of CO_2-rich ice mantles towards several molecular clouds. CO and CO_2 have sharp bands in the infrared and their band shape depends strongly on the ice composition. The profiles of the strong CO and CO_2 bands can therefore provide important information on the composition, temperature and thermal history of interstellar and precometary ices.

We address, in this paper, the infrared spectra of 70 apolar ice mixtures of pure, binary, and multicomponent type. We studied their spectral properties at 10 K, during warm up and UV photolysis, and derived the optical constants. We discuss the importance of particle shape calculations for strong transitions such as CO and CO_2.

In the laboratory context, we investigate the formation of CO_2 in the interstellar medium by UV photolysis of interstellar ices. Together with astronomical spectra taken by the ISO satellite these laboratory data will be extremely valuable for the determination of the grain mantle composition in dense clouds.

Key words: ISM: molecules; dust – infrared: interstellar: lines – methods: laboratory

1. Introduction

Interstellar dust plays an important role in physical and chemical processes in the interstellar medium (ISM). Different dust populations are found in circumstellar envelopes, in the diffuse interstellar medium, and in dense clouds (see Dorschner & Henning 1995 for a review). Interstellar molecular clouds are not homogeneous but show a clumpy structure (Stacey et al. 1993) and offer a variety of environmental conditions. The cold and dense environment in quiescent molecular clouds provides an ideal basis for the accretion of icy grain mantles and coagulation of particles. These clouds evolve from an initial cold, low density and quiescent phase (T=10 K, n = 10^3 cm^{-3}) to warm, dense and active protostellar regions (T=100K, n=10^6 cm^{-3}). Energetic protostellar outflows create shocks which can raise the temperatures locally to more than 2000 K. In these star-formation regions, heating, radiation, and shocks provoke grain processing in the form of desorption, grain explosions, or total grain destruction. Therefore a strong connection is evident between interstellar gas and grain species, which greatly influences both interstellar chemistry and molecular abundances. Grains are exposed to considerable changes during their lifetime while they cycle back and forth between diffuse and dense clouds. Energetic ultraviolet photo-processing of icy grain mantles results in a variety of new molecules and radicals (e.g., d'Hendecourt et al. 1985, Gerakines et al. 1996), which could subsequently re-enter the gas phase. Also, simple molecules which are accreted in dense clouds are converted into complex organics by the UV irradiation in diffuse regions.

Infrared observations toward obscured sources have shown the existence of different grain populations and a variety of molecules which reside on interstellar grains (e.g., Willner et al. 1982, Grim et al. 1991, Whittet et al. 1996). Comparisons of laboratory spectra of astrophysically relevant ice mixtures with interstellar observations have led to first-time detections of solid-state molecules and to studies of gas-grain interactions in interstellar clouds (see reviews by Whittet 1993, Schmitt 1994, d'Hendecourt & Ehrenfreund 1996). Observations to date show that interstellar ices contain H_2O, CO, CH_3OH, CO_2, CH_4, OCS, and some other molecules in lower abundances. Recent observations with the Infrared Space Observatory (ISO) across the entire mid-infrared spectrum allow to study the complete inventory of interstellar ices (Whittet et al. 1996). The nearly ubiquitous presence of CO_2 ice, the low abundance of CH_4 ice, and other important new results are summarized in the ISO Special Issue of Astron. Astrophys. 315 (e.g., de Graauw et al. 1996, Boogert et al. 1996).

Send offprint requests to: P. Ehrenfreund

At low gas densities, theoretical models predict that H_2O-rich ices (which also include small amounts of CO, NH_3 and CH_4) will form on grain surfaces, whereas in high-density environments, grains should accrete mainly apolar molecules from the gas phase (such as CO, N_2, and O_2), with smaller amounts of H_2O. Observational and laboratory-based studies of solid CO have suggested that both polar and apolar ices exist on grain surfaces, presumably arranged in a layered, "onion" structure. The existence of "onion" structures would provide strong constraints on the evolution and life cycles of grains in interstellar clouds (Whittet & Duley 1991, Tielens et al. 1991). Around luminous protostars, apolar ices may be partly evaporated. There is evidence for CH_3OH-rich ice towards the embedded object GL 2136 (Skinner et al. 1992), and recent ISO results show the presence of CO_2-rich ice mantles towards several objects (de Graauw et al. 1996, d'Hendecourt et al. 1996, Ehrenfreund et al. 1997a). Thus towards an embedded object we can observe grain mantles whose compositions reflect the different temperature zones and the line-of-sight conditions.

2. Apolar ices

Apolar ices on interstellar grains are likely composed of molecules such as CO, O_2, N_2 and CO_2. CO is another widespread grain mantle component and has been very well studied by ground-based observations. Detailed studies of the interstellar CO band reveal two components, a narrow band at 2139 cm^{-1} and a broad band at 2136 cm^{-1}, attributed to apolar and polar ices, respectively (Tielens et al. 1991). While the CO abundance towards many sources is estimated at only a few percent relative to H_2O ice, it has been observed at 25 % relative to H_2O in the Taurus dark cloud and as high as 40 % in Serpens (Chiar et al. 1994, 1995). The CO_2 molecule was discovered by d'Hendecourt & de Muizon (1989) in IRAS-LRS spectra of protostars. Re-analysis of LRS spectra has indicated that CO_2 is a wide-spread and very common component in interstellar ices (d'Hendecourt & Ehrenfreund 1996), and the recent results from ISO confirm this (de Graauw et al. 1996). The infrared bands of both CO and CO_2 have been extensively studied in the laboratory by Sandford et al. (1988), Sandford & Allamandola (1990), Palumbo & Strazulla (1993) and Elsila et al. (1997).

Whereas CO and CO_2 have sharp and strong transitions, N_2 and O_2 are homonuclear diatomic molecules which are infrared inactive and radio quiet. Theoretical models suggest that molecules like molecular oxygen and nitrogen are important grain mantle constituents in apolar ices. Thus, apolar ices might serve as a reservoir of interstellar species such as O_2 and N_2, which may only be detected through their subtle influences on the absorption features of other ice constituents, such as CO and CO_2. Despite the fact that these molecules have no innate infrared transitions, interactions with adjacent molecules in the solid state can break the symmetry of their molecular vibrations, and their modes then become weakly infrared active. For instance, the O=O fundamental vibration of O_2 at 1550 cm^{-1} was detected in the laboratory when this molecule was mixed in a CO_2 matrix (Ehrenfreund et al. 1992). Searches for this band in the spectra of interstellar ices at 6.45 μm, as well as for that of solid N_2 at 4.28 μm, are currently underway with ISO. There are at least three more indirect methods which allow to infer the presence of diatomic homonuclear molecules in interstellar ices: (i) their effects on the profiles of CO and CO_2 bands, (ii) the band position of isolated water features, and (iii) their irradiation products (see Ehrenfreund & van Dishoeck 1997 for a review).

Particle size and shape effects can affect an absorption feature. For strong transitions, such as the CO and CO_2 bands, these effects are dominated by surface modes in which the applied electric field polarizes the particle and establishes a surface charge distribution which in turn produces an induced electric field. The strength of this induced field will depend on the optical constants of the material. The absorption by a (molecular) oscillator is then driven by the total electric field which is the sum of both. For very strong transitions such as CO or CO_2, the effects of the induced field can be substantial (cf., Bohren and Huffman 1983; Tielens et al. 1991).

In this paper, we present a study of CO and CO_2 profiles in astrophysically relevant apolar ice mixtures. We have studied the infrared properties of apolar matrices containing CO, N_2, O_2, CO_2 and H_2O (Sects. 4.1 - 4.5). We further address isotopes (Sect. 4.6), multicomponent mixtures (Sect. 4.7), how CO and CO_2 profiles can be used to trace infrared inactive molecules (Sect. 4.8), and the spectral differences between polar and apolar mixtures (Sect. 4.9). The changes in the spectra during warm-up are summarized in Sect. 4.10, and changes upon photolysis are discussed in Sect. 4.11, which also summarizes the CO_2 formation cross section in various matrices. Optical constants and grain shape effects are presented in Sects. 5 and 6. In Sect. 7, we present a "cookbook" approach to guide astronomers in their interpretation of observations of interstellar CO and CO_2 bands. We discuss present day observations of solid CO and CO_2 bands and their implications for the formation and evolution of interstellar ices in Sect. 8. The results are summarized in Sect. 9.

The results are presented as a part of the program at Leiden Observatory dedicated to the solid-state database for ISO. This database of solid CO and CO_2 for ISO can be found on the World Wide Web (WWW) at the URL *http://www.strw.leidenuniv.nl/~ehrenfreund/isodb* and has been active since 1.11.1996 (Ehrenfreund et al. 1996a). It contains 75 experiments on apolar ices and standard polar mixtures. Data files also contain optical constants n and k, and changes in the profiles are simulated for different particle shapes such as spheres, ellipsoids, and core-mantle grains. Also included is a help page for explanations. The database is dynamical and regularly updated. Using this database, observers may attempt to fit their measured profiles themselves, and assess the influence of any particle shape using the optical constants.

3. Experimental

Apolar ices were condensed as pure gases or gas mixtures onto the surface of a CsI window in a high-vacuum chamber and cooled by a closed-cycle He refrigerator to 10 K. Gases were

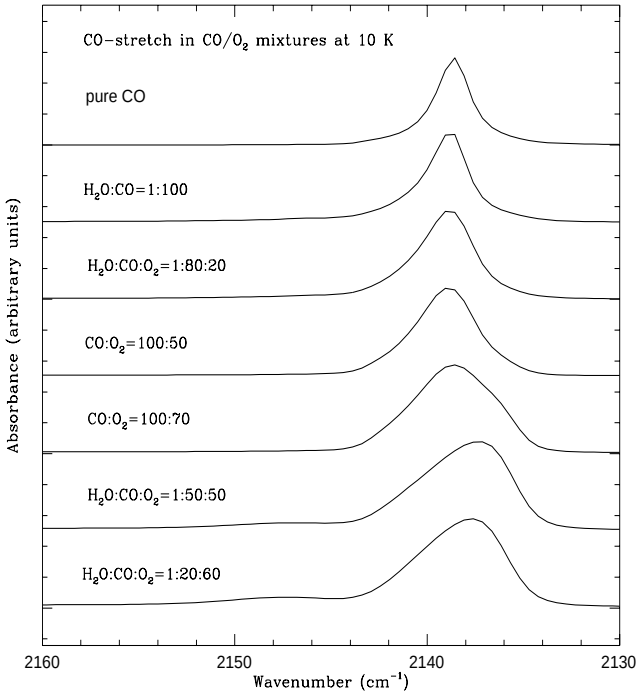

Fig. 1. Infrared absorption spectra of solid CO in CO/O_2 mixtures at 10 K. The band width increases with O_2 concentration, reaching a maximum of 5.5 cm^{-1} when the amounts of CO and O_2 are equal, where the band also shifts by 1.3 cm^{-1} to lower frequency. When O_2 is more abundant in the ice than CO, the band width decreases again. Exact band parameters are listed in Table 1.

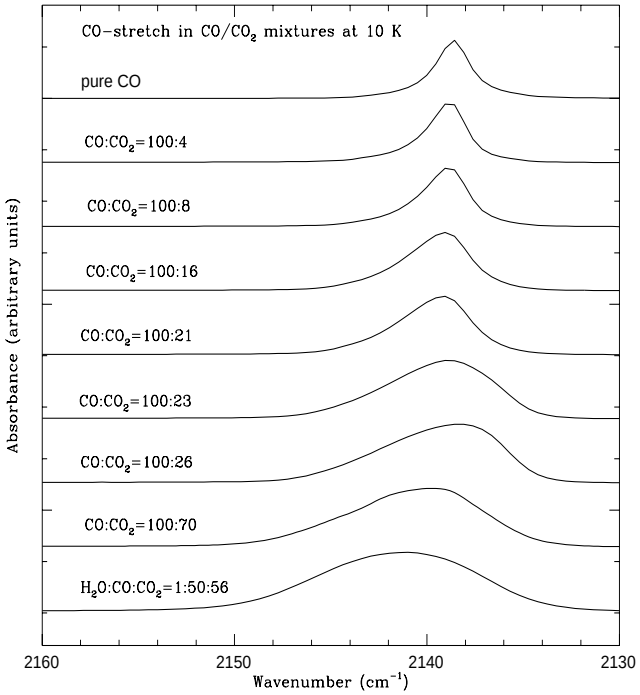

Fig. 2. Infrared absorption spectra of solid CO in CO/CO_2 mixtures. A sharp transition in the CO band width occurs when the amount of CO_2 relative to CO exceeds 21 %. Particular complexes or additonal trapping sites are initiated at such a concentration. This can be used as a sensitive method to determine the amount of CO_2 in apolar interstellar ices.

prepared in a glass vacuum manifold. The purity of the gases CO, CO_2, N_2, and O_2, was 99.9997 % (Messer Griesheim). Infrared transmission spectra were obtained with a BioRad FTS 40A spectrometer at a resolution of 1 cm^{-1}.

UV irradiation was performed using a microwave-excited hydrogen flow lamp. This source has a sharp emission peak at 1216 Å (Lyman α) and additional bands centered at 1360, 1450, 1600 and 2800 Å, which produce a total UV flux of approximately 10^{15} photons cm^{-2} s^{-1} (Weber & Greenberg 1985). The deposition rate and sample thickness growth rate were about 10^{15} molec cm^{-2} s^{-1} and 1 μm hr^{-1}, respectively. Final sample thicknesses ranged from 0.05 to approximately 0.5 μm, depending on the experiment performed. A detailed description of the experimental setup is given by Gerakines et al. (1995). The integrated absorbances of CO, CO_2 and H_2O have been recently calculated by Gerakines et al. (1995) and were used for column density measurements in our experiments.

4. Results

4.1. Laboratory spectroscopy

The variations in peak position, full width at half maximum (FWHM), and profile structure of the CO and CO_2 infrared absorption bands are the result of a complex interplay between the molecules present in the ice matrix, which includes dispersive, electrostatic, induced, and repulsive interactions (Barnes et al. 1980). Variations occur during warm-up and UV irradiation of the ice mixtures. In apolar matrices, the interactions are controlled by dispersive and repulsive forces, and the measured shift in peak position scales approximately with the polarizability. However, the exact position and profile of a band is determined by the physical and chemical interactions with the surrounding molecules. Broadening of features is caused by interactions with neighbours and the presence of a distribution of trapping sites. The nature of interactions in molecular solids also determines band shifts as compared to the gas phase. Repulsive and attractive forces both occur in ice matrices at the same time and their relative intensities determine the crystal shape and size. The fundamental vibration of molecules in a matrix are in general red-shifted from the gas-phase value.

Pure CO gas absorbs at 2143.3 cm^{-1}. Gas-phase CO_2 peaks at 2349 cm^{-1} in the stretching mode and 667.4 cm^{-1} in the bending mode. The fundamental transitions of the infrared-inactive molecules O_2 and N_2 fall at 1551 cm^{-1} and 2335 cm^{-1}, respectively. In the solid state, these modes become weakly infrared active due to interactions with surrounding molecules (Ehrenfreund et al. 1992).

Sandford et al. (1988) demonstrated that the exact position, width, and profile of the solid-state CO absorption feature near 2140 cm^{-1} is extremely sensitive to the physical conditions

Table 1. Band position and width (in cm^{-1}) of the CO-stretch in CO/O_2 matrices.

	^{12}CO stretch		
	Position	FWHM	
Ice composition	cm^{-1}	cm^{-1}	T
pure CO	2138.7	2.2	10 K
pure CO	2138.8	2.1	30 K
H_2O:CO=1:100	2138.9	2.6	10 K
H_2O:CO=1:100	2138.9	2.5	30 K
H_2O:CO:O_2=1:80:20	2138.8	3.4	10 K
H_2O:CO:O_2=1:80:20	2138.8	3.2	30 K
CO:O_2=100:50	2138.9	3.8	10 K
CO:O_2=100:50	2138.8	3.1	30 K
CO:O_2=100:70	2138.6	5.2	10 K
H_2O:CO:O_2=1:50:50	2137.4	5.5	10 K
H_2O:CO:O_2=1:50:50	2139.0	4.3	30 K
H_2O:CO:O_2=1:20:60	2137.8	5.0	10 K
H_2O:CO:O_2=1:20:60	2139.4	4.7	30 K

present during the ice accretion phase as well as any subsequent thermal processes and radiation exposure. The observed variations in the peak position and width of the 2140 cm^{-1} feature also reflect variations in the composition, size distribution, and shape distribution of the grains. N_2 and CO have identical crystalline structures at low temperatures and nearly equal site dimensions (Hagen & Tielens 1981). Therefore CO and N_2 co-crystallize easily and preferentially on a local scale. This might not be the case for CO and O_2, depending upon the particular shape of O_2. The CO_2 molecule builds preferentially interactions in the form of T-shaped complexes. In general, the presence of O_2 or CO_2 in a CO matrix invokes strong perturbations, resulting in frequency shifts and broadening of the CO band (Ehrenfreund et al. 1996b).

Laboratory studies have shown that the CO_2 molecule is formed readily upon UV irradiation of ices containing both H_2O and CO (d'Hendecourt et al. 1986). Sandford & Allamandola (1990) have shown that the FWHM of the asymmetric stretching mode of CO_2 ranges from 4.7 to 30 cm^{-1} in different ice mixtures, and that the peak position also varies. CO_2 in high concentrations prevents other molecules from forming a complete lattice and mediates the overall molecular structure. Ices in dense interstellar clouds are most likely condensed in amorphous form as there is insufficient energy at these low temperatures to permit rearrangements. The overall composition of the matrix and its temperature determines the interaction and the molecular site geometry (Sandford et al. 1988). During annealing (warm-up) the matrix is rearranged into more energetically favoured orientation and molecules partly diffuse through the matrix. Micro-crystalline structures grow, leading to a sharpening of some bands. Some spectacular examples are given in Figs. 10, 11, and 15. For a detailed description of physical and chemical interactions as well as complex formation in apolar ice matrices the reader is referred to Ehrenfreund et al. (1997b).

4.2. CO/O_2 matrices

Fig. 1 shows infrared absorption spectra of solid CO in CO/O_2 mixtures at 10 K, and the parameters of the CO band in these mixtures at both 10 and 30 K are summarized in Table 1. Some experiments contain H_2O ice on the 1 % level and were performed in order to characterize the "isolated water" bands (Ehrenfreund et al. 1996b). The CO band position remains rather stable, with a maximum redshift of 1.3 cm^{-1} when O_2 is equally abundant to CO. The continuous increase in width of the CO band with increasing O_2 concentration reveals the build-up of $CO:O_2$ complexes or additional trapping sites. These perturbations lead to a fragile matrix structure which can be monitored as a rapid decrease of band width during slight warm-up when ices are rearranged (see Table 1).

4.3. CO/CO_2 matrices

Spectra of the CO and CO_2 stretching modes are shown in Figs. 2 and 3. CO_2 forms complexes not only with itself, but with a variety of other species, and so its presence influences their band profiles as well. This is particularly pronounced for the CO fundamental (cf. Fig. 2). A large increase in FWHM (3 cm^{-1}) is observed when the concentration of CO_2 relative to CO in the mixture changes from 21 to 26 %, indicating the importance of aggregate formation induced by the presence of CO_2.

CO_2 has five active bands in the mid-infrared, which have been described in detail by Sandford & Allamandola (1990). In Fig. 3 we show the behavior of the CO_2 symmetric stretching mode. This feature, which falls at 2340 cm^{-1}, is rather unique in a pure CO_2 ice; at T=10 K it has a large FWHM and wings on both the high and low frequency side (see Fig. 3). Like the CO band, the CO_2 stretch also shows a remarkable "jump" in width in the interval between CO_2:CO = 21 - 26 % (2.2 cm^{-1}). The CO-CO_2 interactions lead, with increasing concentration of CO_2, to an enormous width of 20 cm^{-1} for this feature, comparable to that of polar mixtures. It is important to emphasize, therefore, that a large band width is not only characteristic of polar mixtures. In contrast to the CO band, the CO_2 band's position shifts with increasing CO_2 concentration to lower frequencies, reflecting an overall more attractive interaction in the matrix for CO_2 than for CO.

In Fig. 4 we display the CO_2 bending fundamental near 650 cm^{-1} (15.2 μm). This vibration is doubly degenerate, and the band splits when the axial symmetry of the molecule is broken. Pure CO_2 shows a clear double-peaked structure in the bending mode (Sandford & Allamandola 1990). The band position, width, and shoulders due to complexes are given in Table 2. The double-peaked structure is unique to pure and annealed CO_2, and merely a broad band is observed when CO_2 is a part of an ice mixture. An increasing concentration of CO_2 reveals CO-CO_2 complexes or second trapping sites, which appear in low CO_2 concentrations as a shoulder, and thereafter as a broad band, which shifts slightly to lower frequencies.

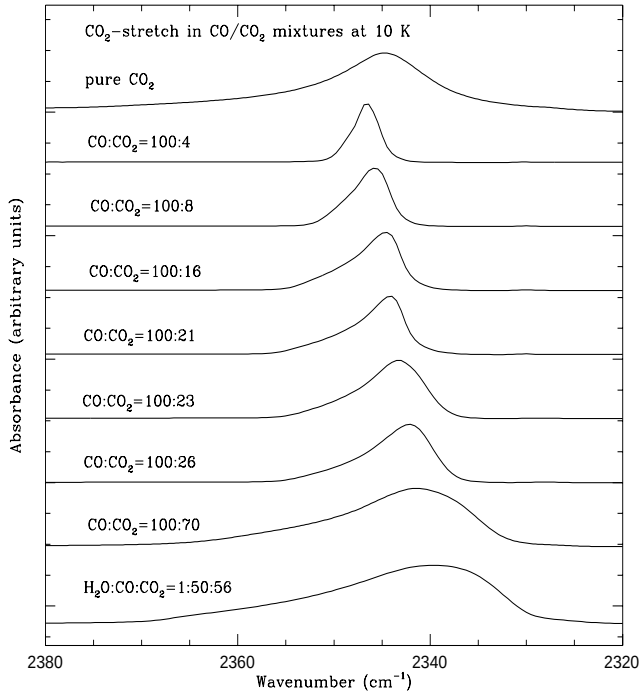

Fig. 3. Infrared absorption spectra of the stretching mode of solid CO_2 in CO/CO_2 mixtures. A very large band with strong red and blue wings is characteristic for pure CO_2, reflecting the strong interactions between CO_2 molecules. A gradual shift in peak position to lower frequencies as well as a gradual increase in the band width is evident with increasing concentrations of CO_2. Band width reaches its maximum of 19 cm^{-1} at equal abundances of CO and CO_2.

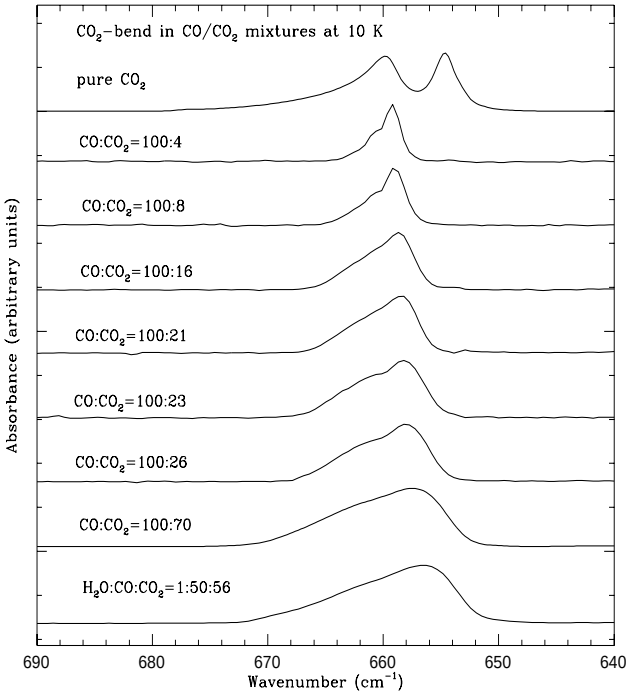

Fig. 4. Infrared absorption spectra of the bending mode of solid CO_2 in CO/CO_2 mixtures. The double-peaked structure is unique to pure and annealed CO_2. A single band is observed in CO_2 mixtures, but complexes or additional trapping sites produce shoulders at low CO_2 concentrations and a large width at higher CO_2 concentrations.

The ^{13}CO band at 2090 cm^{-1} is shown in Fig. 5. In comparison with Fig. 2, it is observed that the isotope ^{13}CO behaves in a somewhat similar fashion, but not exactly the same, as ^{12}CO. The ^{13}CO band has an intrinsic strength which is similar to that of ^{12}CO (1.3×10^{-17} cm molec^{-1}; Gerakines et al. 1995), but the low isotopic abundance of ^{13}C relative to ^{12}C makes this feature difficult to observe in interstellar ices. The $^{13}CO_2$ asymmetric stretching fundamental (ν_3) falls at 2280 cm^{-1} and is displayed in Fig. 6. In comparison with Fig. 3, it is evident that the behavior of these two isotopes is rather different.

CO_2 readily forms specific complexes with other species. The $^{12}CO_2$ band is known to show a unique structure and large band width of 12 cm^{-1}. In contrast, the $^{13}CO_2$ band is very narrow (2.6 cm^{-1}), which has already been discussed by Sandford & Allamandola (1990). The changes in spectral signature are due to differences in the induced dipole moment or some decoupling of the $^{13}CO_2$ molecules from the $^{12}CO_2$ phonon modes. $^{13}CO_2$ has also a much lower abundance than $^{12}CO_2$ and is therefore exposed to very different interactions in the ice, which may also result in a different infrared signature (Ehrenfreund et al. 1997b). This has important implications for astronomy, see also Sect. 4.6.

4.4. CO/O_2/CO_2 matrices

Figs. 7 and 8 display the behavior of the CO and CO_2 stretching modes in $CO/O_2/CO_2$ matrices. The band widths of CO and CO_2 are, with a few exceptions, comparable in these mixtures. The band width of the CO feature seems to be determined by the interactions between O_2 and CO_2. Fig. 7 shows the influence of these particular O_2-CO_2 perturbations which have been already observed by Ehrenfreund et al. (1996b). Band parameters at 10 and 30 K are shown in Table 3, including additional mixtures which are not displayed in Figs. 7 and 8.

The CO band width in a $CO:O_2$=100:50 mixture was measured to be 3.8 cm^{-1} (Sect. 4.2, see Table 1), but an additional interaction is induced by the CO_2 molecule into the ice mixture, resulting in a further increase of band width. This increase may be inferred from the band width of CO in binary mixtures listed in Tables 1 and 2. Strong differences in peak position and band width after warm-up to 30 K reflect loose aggregates between the ice constituents which are rearranged during the rise temperature. The measured column densities of CO and CO_2 remained constant at 10 K and 30 K, indicating that no sublimation has yet occured. The variety of interactions in multicomponent mixtures and the difficulty in extracting information are each shown in Fig. 7, where the mixtures $CO:O_2:CO_2$=100:20:11 and $CO:O_2:CO_2$=100:11:20, which are similar in composition, show very different band profiles. On the contrary the mixtures $CO:O_2:CO_2$=100:50:21 and $CO:O_2:CO_2$=100:11:20 show

Table 2. Band position and width (in cm^{-1}) of CO and CO_2 IR absorption features in CO/CO_2 matrices. (s) indicates band shoulders.

	^{12}CO stretch		$^{12}CO_2$ stretch		$^{12}CO_2$ bend		
	Position	FWHM	Position	FWHM	Position	FWHM	
Ice composition	cm^{-1}	cm^{-1}	cm^{-1}	cm^{-1}	cm^{-1}	cm^{-1}	T
$CO:CO_2$=100:4	2138.8	2.5	2346.7	3.1	659.2/660.8(s)	2.5	10 K
$CO:CO_2$=100:4	2138.8	2.3	2346.6	3.6	659.4/660.8	3.3	30 K
$CO:CO_2$=100:8	2138.9	3.0	2345.9	4.4	658.9/660.8(s)	3.5	10 K
$CO:CO_2$=100:8	2138.8	2.7	2345.8	4.5	659.2/660.8	4.0	30 K
$CO:CO_2$=100:16	2139.1	3.8	2344.6	5.4	658.7	5.3	10 K
$CO:CO_2$=100:16	2139.0	3.7	2344.5	5.3	658.7	5.4	30 K
$CO:CO_2$=100:21	2139.2	4.4	2344.2	5.3	658.4	6.2	10 K
$CO:CO_2$=100:21	2139.2	4.1	2344.2	5.3	658.5/660.8	6.2	30 K
$CO:CO_2$=100:23	2138.9	6.4	2343.4	7.7	658.3/660.8(s)	7	10 K
$CO:CO_2$=100:23	2139.2	4.6	2344.1	5.3	658.5	6.3	30 K
$CO:CO_2$=100:26	2138.4	7.4	2342.3	7.5	658.0/661.3(s)	7.4	10 K
$CO:CO_2$=100:26	2139.3	4.5	2343.9	5.3	658.1	6.7	30 K
$CO:CO_2$=100:70	2139.9	8.2	2341.4	14.8	657.6	10.6	10 K
$H_2O:CO:CO_2$=1:50:56	2141.3	9.6	2339.7	19.1	656.6	10.2	10 K
$H_2O:CO:CO_2$=1:50:56	2141.3	7.9	2342.8	9.4	655.5/661.0	10.3	45 K

Table 3. Band positions and widths (in cm^{-1}) of CO and CO_2 IR absorption features in $CO/O_2/CO_2$ matrices. (s) indicates band shoulders.

	^{12}CO stretch		$^{12}CO_2$ stretch		$^{12}CO_2$ bend		
	Position	FWHM	Position	FWHM	Position	FWHM	
Ice composition	cm^{-1}	cm^{-1}	cm^{-1}	cm^{-1}	cm^{-1}	cm^{-1}	T
$CO:O_2:CO_2$=100:50:4	2138.9	4.4	2346.3	4.9	658.7/661(s)	4.9	10 K
$CO:O_2:CO_2$=100:50:4	2139.4	4.3	2346.6	3.2	658.9/660.9	5.0	30 K
$CO:O_2:CO_2$=100:50:8	2138.1	6.0	2344.2	5.3	658.7/661.3(s)	6	10 K
$CO:O_2:CO_2$=100:50:16	2137.9	6.3	2342.9	6.3	658.3/661.3(s)	7.2	10 K
$CO:O_2:CO_2$=100:50:16	2139.2	4.8	2345.6	5.6	658.2/660.8/662.7	7.0	30 K
$CO:O_2:CO_2$=100:50:21	2138.1	6.5	2342.5	6.3	658.3/661.5(s)	7.7	10 K
$CO:O_2:CO_2$=100:50:21	2139.1	4.7	2345.0	8.0	657.5/660.8/662.7	9.6	30 K
$CO:O_2:CO_2$=100:50:32	2138.9	7	2342.1	6.7	658.2/662.2(s)	8.8	10 K
$CO:O_2:CO_2$=100:54:10	2137.6	5.6	2343.5	5.4	658.5/661.5(s)	7	10 K
$CO:O_2:CO_2$=100:54:10	2139.1	3.7	2346.2	4.3	658.5/660.7	5.6	30 K
$CO:O_2:CO_2$=100:20:11	2139.1	4.7	2345.8	5.9	658.7/660.7(s)	5.3	10 K
$CO:O_2:CO_2$=100:20:11	2139.4	4.5	2345.9	6.0	659.0/660.8/662.5	5.4	30 K
$CO:O_2:CO_2$=100:11:20	2138.3	6.7	2342.8	7	658.3/661.7(s)	7.2	10 K
$CO:O_2:CO_2$=100:11:20	2139.6	5	2344.8	7	658.5	6.5	30 K
$CO:O_2:CO_2$=100:10:23	2138.3	7.2	2342.4	7.3	658.2/661.7(s)	7.7	10 K
$CO:O_2:CO_2$=100:10:23	2139.2	4.6	2344.2	5.2	658.2	6.3	30 K

Table 4. Band position and width (in cm^{-1}) of CO_2 IR absorption features in CO_2/H_2O matrices. The last column lists the peak ratio of the double-peaked CO_2 bending mode.

	$^{12}CO_2$ stretch		$^{12}CO_2$ bend		T	Intensity ratio
Ice composition	Position	FWHM	Position	FWHM		655/660
	cm^{-1}	cm^{-1}	cm^{-1}	cm^{-1}		cm^{-1}
pure CO_2	2344.8	12.2	654.7/659.9	2.6/4.7	10 K	1.051
pure CO_2	2344.9	11.7	654.7/659.7	2.5/3.8	50 K	0.998
pure CO_2	2344.6	9	654.9/660.1	1.6/2.8	80 K	0.889
$CO_2:H_2O$=100:1	2345.0	14.1	654.0 /659.9	2.5/5.1	10 K	1.00
$CO_2:H_2O$=100:1	2344.8	15.1	654.7/659.6	2.0 /5.1	30 K	1.00
$CO_2:H_2O$=10:1	2330.1	28.6	655.1	11.0	10 K	-
$CO_2:H_2O$=10:1	2343.9	7.4	654.0 /660.0	2.5/3.6	80 K	0.969
$CO_2:H_2O$=6:1	2332.2	31	655.5	12.3	10 K	-
$CO_2:H_2O$=6:1	2343.9	8.5	654.8/660.0	3.0 /4	80 K	1.026

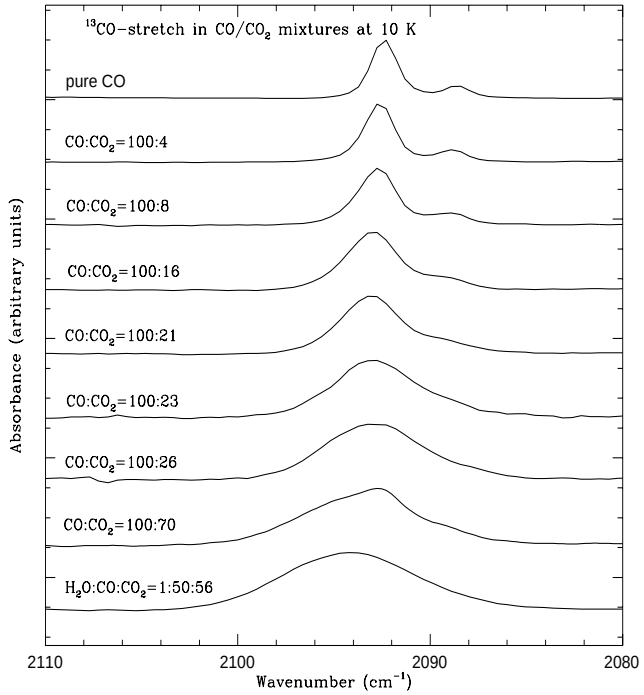

Fig. 5. Infrared absorption spectra of solid ^{13}CO in CO/CO_2 mixtures. This isotope shows a similar behavior compared to the fundamental mode of ^{12}CO at 2140 cm^{-1} and is characterized by a rather stable peak position and increase in width. However, the increase in band width does not exactly follow that of ^{12}CO, since ^{13}CO is only a minor constituent and exposed to different interactions.

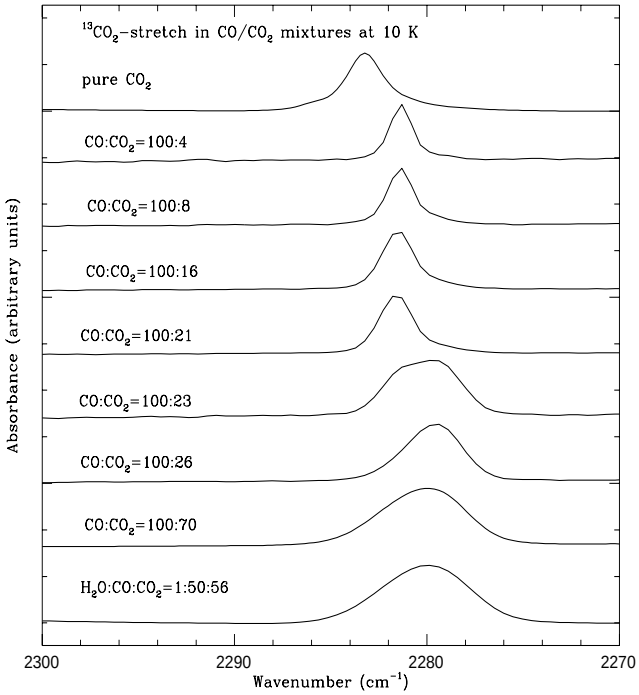

Fig. 6. Infrared absorption spectra of solid $^{13}CO_2$ in CO/CO_2 mixtures. This isotope shows a different behavior and is much narrower than the band of $^{12}CO_2$ at 2340 cm^{-1} (compare Fig. 3). A strong plateau is visible when the concentration of CO_2:CO exceeds 21 %, indicating a complex formation, which can also be observed for $^{12}CO_2$, see Fig. 3.

very similar spectroscopic properties, indicating that the relative abundance of O_2 and CO_2 molecules determines width and band position of the CO and CO_2 bands. Fig. 8 shows the behavior of the CO_2 stretching mode and the blueshift which is observed in matrices where interactions between those molecules are reduced (CO_2 and O_2 are less abundant in the ice). The interactions between CO, O_2 and CO_2 also result in several sub-peaks which appear superimposed on the bending mode of CO_2 and are listed in Table 3 (see also Ehrenfreund et al. 1996a).

4.5. CO_2/H_2O mixtures

CO_2/H_2O mixtures reveal an outstanding behaviour and have a strong effect on the CO_2 band profiles, which is of extreme importance for the abundance determinations and studies of interstellar CO_2. When the amount of water ice in a CO_2/H_2O ice mixture exceeds a few percent, very strong aggregates and additional trapping sites are formed which lead to a very peculiar profile of the CO_2 stretching mode (Ehrenfreund et al. 1997b). In Fig. 9, it is shown that a second band appears at 2328 cm^{-1}, which results in an enormous broadening of the band (FWHM = 30 cm^{-1}) and an asymmetric profile which is shifted by about 15 cm^{-1} to lower frequency. This particular profile remains constant even to equal concentrations of CO_2 and H_2O. In polar mixtures, where H_2O is more abundant in the ice matrix, the band position peaks again around 2341 cm^{-1} (close to that of pure CO_2), and the FWHM is reduced to 15 cm^{-1}, see Sect. 4.9. The bending mode (Fig. 11) shows a similar behavior. A constant profile is observed in mixtures where CO_2:H_2O = 10:1, 10:6 and 1:1, which is also characterized by a large band width (12 cm^{-1}) and a strong redshift. Band parameters are given in Table 4.

Stepwise annealing of a CO_2:H_2O=6:1 mixture revealed different components which form this unusually large and asymmetric band profile (see Fig. 10). The band of pure CO_2 (at 2344 cm^{-1}) can be distinguished only at temperatures above 42 K. At low temperature, the peak at 2328 cm^{-1}, which is likely due to a second trapping site for CO_2 induced by the matrix configuration, dominates the CO_2 profile. This trapping site is destroyed during warm-up between 42 and 50 K. At 75 K, the band shows a profile similar to that of pure CO_2. Rearrangement of the ice matrix during the annealing process separates the CO_2 and H_2O molecules, which thereafter reside within the same ice matrix in a two-phase system.

Spectroscopy of the bending mode of solid CO_2 in a CO_2:H_2O=6:1 mixture during warm-up, shown in Fig. 11, reveals how the matrix is rearranged during annealing. A conversion of the asymmetric band into one resembling that of pure CO_2 occurs at the same temperature as for the stretching mode, showing the typical double-peaked structure. CO_2/H_2O ices show a unique behavior which is easy to distinguish from other ice mixtures containing CO_2. However, the same band po-

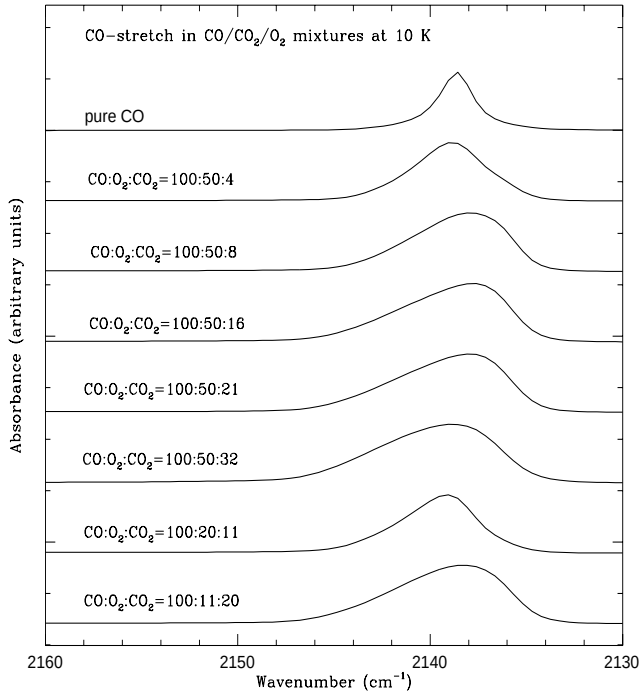

Fig. 7. Infrared absorption spectra of solid CO in $CO/O_2/CO_2$ mixtures. The peak position remains constant within 1.5 cm^{-1}, and the band width varies from 4.3 cm^{-1} to 7.2 cm^{-1}.

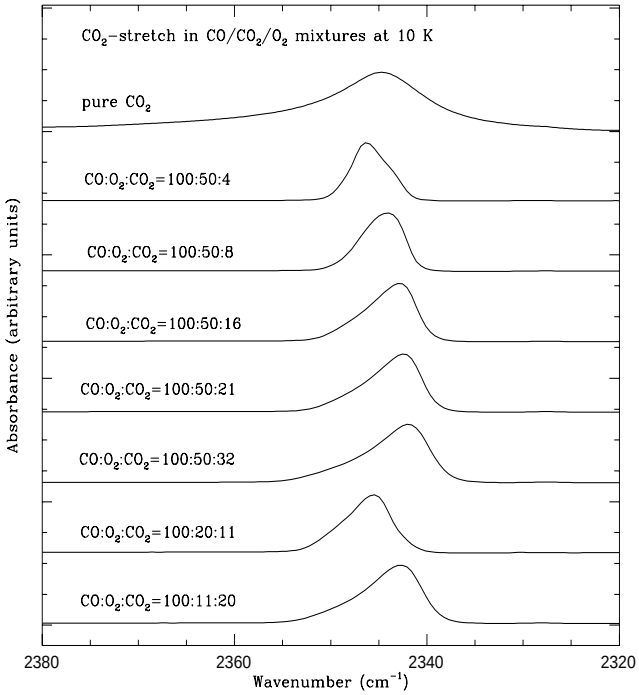

Fig. 8. Infrared absorption spectra of solid CO_2 in $CO/O_2/CO_2$ mixtures. A gradual redshift is observed for increasing concentration of CO_2 (4 cm^{-1}). The width varies from 4.9 cm^{-1} to 7.3 cm^{-1}, as for the CO band (Fig. 7).

sition is observed for ices with an H_2O abundance relative to CO_2 in the range of 10 - 50 %, making it difficult to determine the exact H_2O content. The two peaks, shown in Fig. 11 at 42 K, can only be distinguished when H_2O ice is less abundant than 10 % relative to CO_2. Except pure CO_2 only annealed ice mixtures display the specific double-peaked structure, as discussed in Sect. 4.1. It is interesting to note that the the band widths of the CO_2 bending mode are different in "annealed" samples of pure CO_2 and those of CO_2 embedded in a mixture (see Table 4). Small changes in the peak ratio of the double peak are listed in Table 4. The band positions, however, remain constant (see Table 4). This is of particular importance for astronomical observations, see Sect. 8.

4.6. Isotopes

High signal to noise spectra are required to accurately measure the $^{12}C/^{13}C$ ratio of the CO_2 bands near 2340 cm^{-1} and 2280 cm^{-1}. This ratio is of much interest for models of the chemical evolution of the galaxy, and the strong transition of $^{13}CO_2$ has already revealed preliminary $^{13}CO_2/^{12}CO_2$ ratios towards several interstellar targets (de Graauw et al. 1996, d'Hendecourt et al. 1996). Sandford & Allamandola (1990) have shown that the relative strengths of the isotopic CO_2 bands vary slightly in different matrices but are constant and temperature independent within a given matrix. As seen from Fig. 6, the $^{13}CO_2$ band behaves rather differently than that of $^{12}CO_2$. Therefore observations of $^{12}CO_2$ and $^{13}CO_2$ bands can provide two virtually independent tests for the ice composition. In Table 5, we list the isotopic ratios (ratio of the integrated band intensities) of 24 mixtures. Assuming that the $^{13}CO_2/^{12}CO_2$ ratio in our experiments has a terrestrial value of 0.0112 ($\frac{1}{89}$), it is possible to derive the correction coefficients for each ice matrix. The deviations of the $^{13}CO_2/^{12}CO_2$ ratio from the terrestrial value are between -10 and +20 %. The strongest deviations (up to +20 %) are observed in mixtures that show broad CO_2 profiles and where strong interactions in the matrix are evident. Whereas errors of ± 3 % could be introduced by measurement inaccuracies, the remaining discrepancies are not determined. Two possible explanations could be that (i) near strong transitions, the refractive index n is very large, or that (ii) the band strength depends on the specific matrix composition.

Band parameters of $^{13}CO_2$ and of the CO_2 combination modes are listed in Table 6. The (ν_1 + ν_3) mode occurs near 3700 cm^{-1}, and the ($2\nu_2$ + ν_3) band falls near 3600 cm^{-1}. Both bands are relatively strong (1.4×10^{-18} and 4.5×10^{-19} cm molec^{-1}; Gerakines et al. 1995) and follow in general the trends of the $^{12}CO_2$ stretch.

4.7. Multicomponent mixtures

The behavior of the CO profile in multicomponent mixtures varies strongly, see Fig. 12 and corresponding Table 7. As already explained in Sect. 4.4, the presence of large amounts of CO_2 and O_2 are responsible for a strong broadening of the CO band, as well as extensive shifts in peak position. The pres-

Table 5. Isotopic ratio of $^{13}CO_2/^{12}CO_2$ in various matrices. The terrestrial $^{13}C/^{12}C$ ($^{12}C/^{13}C$) ratio is defined as 0.0112 (89)

Ice matrix	$^{13}C/^{12}C$	$^{12}C/^{13}C$
pure CO_2	0.01103	90.7
H_2O:CO_2=1:100	0.0112	89.3
H_2O:CO_2=1:10	0.0135	74.1
H_2O:CO_2=1:6	0.01268	78.9
CO:CO_2=100:4	0.01015	98.5
CO:CO_2=100:8	0.0102	98.0
CO:CO_2=100:16	0.01012	98.8
CO:CO_2=100:21	0.01014	98.6
CO:CO_2=100:23	0.01049	95.3
CO:CO_2=100:26	0.01037	96.4
H_2:O:CO:CO_2=1:50:56	0.01231	81.2
CO:O_2:CO_2=100:50:4	0.01008	99.2
CO:O_2:CO_2=100:50:8	0.01008	99.2
CO:O_2:CO_2=100:50:16	0.01034	96.7
CO:O_2:CO_2=100:50:21	0.00997	100
CO:O_2:CO_2=100:50:32	0.0102	98.0
CO:O_2:CO_2=100:54:10	0.01010	99.0
CO:O_2:CO_2=100:20:11	0.00992	101
CO:O_2:CO_2=100:11:20	0.01010	99.0
CO:O_2:CO_2=100:10:23	0.01053	95.0
CO:N_2:CO_2=100:50:20	0.0103	97.1
CO:O_2:N_2:CO_2=100:50:25:32	0.01023	97.8
H_2O:CO:O_2:N_2:CO_2=1:50:35:15:3	0.00999	100
H_2O:CO:O_2:N_2:CO_2=1:25:25:10:13	0.01056	94.7

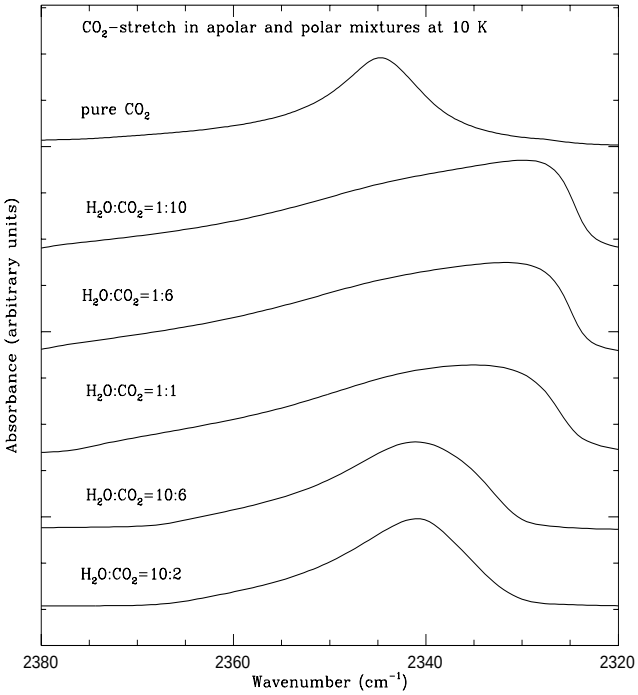

Fig. 9. Infrared spectra of the solid CO_2 stretching mode in CO_2/H_2O mixtures. A rather peculiar profile is observed for the CO_2 stretch, which is shifted to lower frequency and characterized by a large band width, the largest observed in the 60 mixtures studied. Particular aggregates and additional trapping sites are formed between these two molecules when the H_2O abundance exceeds 10 % relative to CO_2. The profile remains constant until equal concentration of CO_2 and H_2O are reached. In polar mixtures, the band position shifts again close to the frequency of pure CO_2 (2344 cm^{-1}) and the band width decreases.

ence of the N_2 molecule has only a small effect on the CO profile. In large concentrations N_2 does, however, invoke a small blueshift of the CO band ($\sim 1\ cm^{-1}$). The band width is hardly affected (see Fig. 12). The behavior of CO_2 bands in multicomponent mixtures is very diverse and has already been discussed by Ehrenfreund et al. (1996a).

4.8. CO and CO_2 as probes of solid O_2 and N_2

The fundamental vibrations of O_2 and N_2 are very weak, and it is not certain if these features will ever be detected in space. Even so, the influence of these molecules on the profiles of strong bands, such as those of CO and CO_2, could be used to infer their presence and relative abundances. In Fig. 13, it is shown that the CO_2 band in a CO_2:O_2=1:1 mixture is very broad (16.5 cm^{-1}) and strongly redshifted from the band position of pure CO_2. With the exception of this mixture, such a strong redshift is only observed (out of 30 mixtures studied) in CO_2:H_2O ices which show some other distinguishing characteristics (see Sect. 4.5). CO_2 and O_2 have strong interactions, which have been already discussed by Ehrenfreund et al. (1996b). These perturbations, resulting in rather particular band shapes (see Fig. 13), could be used to trace solid molecular oxygen. The molecule N_2 is a "silent" matrix component, leading to small blueshifts only. Elsila et al. (1997) have investigated the CO profile in apolar mixtures and claim that best matches with the narrow interstellar CO band can be achieved with laboratory mixtures containing comparable amounts of N_2, O_2, CO_2 and CO. Combined analyses of the CO and CO_2 stretching and bending mode profiles will provide a powerful method of tracing infrared-inactive molecules (see also Ehrenfreund & van Dishoeck 1997).

4.9. CO in polar/apolar mixtures

Fig. 14 illustrates the differences in CO band profiles in polar and apolar ice mixtures. Within polar mixtures, the CO band profile remains rather constant. It is important to note that a broad CO band could also arise from apolar mixtures, e.g. when CO_2 is present in concentrations above 22 % relative to CO (see Sect. 4.3).

A shoulder centered near 2150 cm^{-1} is observed in all polar ice mixtures containing CO. This band has been described in great detail by Sandford et al. (1988). The authors attribute this feature to interstitial CO (in between host molecules), located within the pores of the amorphous H_2O lattice. The interstitial sites, which absorb at 2150 cm^{-1}, are certainly less stable than the sites which absorb at 2140 cm^{-1}, and are only present in H_2O-rich ices which have not experienced warm-up or strong UV irradiation. Schmitt et al. (1989) assigned the 2150 cm^{-1} feature to hydrogen-bonded CO-H_2O complexes in water ice. Jenniskens et al. (1995) also assign this band to CO-H_2O com-

Table 6. Band positions and widths (in cm^{-1}) of $^{13}CO_2$ and the CO_2 combination modes at 10 K.

	$^{13}CO_2$ stretch		$^{12}CO_2$ ($\nu_1 + \nu_3$)		$^{12}CO_2$ ($2\nu_2 + \nu_3$)	
	Position	FWHM	Position	FWHM	Position	FWHM
Ice composition	cm^{-1}	cm^{-1}	cm^{-1}	cm^{-1}	cm^{-1}	cm^{-1}
pure CO_2	2283.3	2.6	3708.9	2.6	3600.3	1.9
H_2O:CO_2=1:100	2283.2	2.6	3708.7	2.5	3600.2	1.8
H_2O:CO_2=1:10	2280.4	7.4	3703.8	11.5	3596.7	8.3
H_2O:CO_2=1:6	2280.3	7.5	3704.0	11.0	3596.6	8.7
CO:CO_2=100:4	2281.3	1.6	3708.1	2.3	3602.3	2.3
CO:CO_2=100:8	2281.3	1.9	3708.2	2.5	3602.3	2.5
CO:CO_2=100:16	2281.4	2.0	3708.3	2.9	3602.4	2.9
CO:CO_2=100:21	2281.7	2.0	3708.5	3.2	3602.5	3.0
CO:CO_2=100:23	2279.8	4.4	3705.9	5.8	3600.0 /3602.1	7.5
CO:CO_2=100:26	2279.6	3.5	3705.7	4.5	3600.0	3.4
H_2:O:CO:CO_2=1:50:56	2279.9	5.6	3705.9	6.6	3599.6	5.7
CO:O_2:CO_2=100:50:4	2281.0 /2279.4	4	3708.0 /3705.6	5.3	3602.0 /3599.7	4.3
CO:O_2:CO_2=100:50:8	2279.2	3.7	3705.2	4.3	3599.8	3.0
CO:O_2:CO_2=100:50:16	2279.1	3.2	3705.2	3.8	3599.8	3.1
CO:O_2:CO_2=100:50:21	2279.1	3.4	3705.0	4.0	3599.7	3.3
CO:O_2:CO_2=100:50:32	2279.3	3.7	3705.4	4.4	3599.9	3.7
CO:O_2:CO_2=100:54:10	2279.1	3.2	3705.1	3.8	3599.7	3.0
CO:O_2:CO_2=100:20:11	2281.5	2.1	3708.4	2.9	3602.4	2.9
CO:O_2:CO_2=100:11:20	2279.6	3.6	3705.7	4.5	3600.0	3.5
CO:O_2:CO_2=100:10:23	2279.5	3.5	3705.7	4.3	3599.9	3.5
CO:N_2:CO_2=100:50:20	2281.9	2.0	3709.2	3.1	3603.5	3.2
CO:O_2:N_2:CO_2=100:50:25:32	2279.5	3.5	3705.9	4.4	3600.5	3.8
H_2O:CO:O_2:N_2:CO_2=1:50:35:15:3	2279.3	3.1	3705.2	4.1	3600.1	2.6
H_2O:CO:O_2:N_2:CO_2=1:25:25:10:13	2279.4	4.0	3705.8	5.4	3600.6	4.4

Table 7. Band positions and widths (in cm^{-1}) of CO and CO_2 IR absorption features in multicomponent matrices. (s) indicates band shoulders.

	^{12}CO stretch		$^{12}CO_2$ stretch		$^{12}CO_2$ bend		
	Position	FWHM	Position	FWHM	Position	FWHM	
Ice composition	cm^{-1}	cm^{-1}	cm^{-1}	cm^{-1}	cm^{-1}	cm^{-1}	T
H_2O:CO:N_2=1:50:50	2139.3	2.7	-	-	-	-	10 K
H_2O:CO:N_2=1:50:50	2139.4	2.8	-	-	-	-	30 K
CO:O_2:N_2=100:50:25	2139.1	3.4	-	-	-	-	10 K
CO:O_2:N_2=100:50:25	2139.1	3.2	-	-	-	-	30 K
H_2O:CO:O_2:N_2=1:40:40:15	2139.1	5.0	-	-	-	-	10 K
H_2O:CO:O_2:N_2=1:40:40:15	2139.1	3.9	-	-	-	-	30 K
CO_2:O_2=1:1	-	-	2338.2	16.5	658.0	12	10 K
CO:N_2:CO_2=100:50:20	2139.7	4.2	2345.7	6.5	659.4	6	10 K
CO:N_2:CO_2=100:50:20	2139.6	4.4	2346.0	6.7	659.2	6.0	30 K
CO:O_2:N_2:CO_2=100:50:25:32	2139.0	7	2342.5	7	658.5/662.4(s)	8.4	10 K
CO:O_2:N_2:CO_2=100:50:25:32	2139.1	7.3	2343.2	8.6	658.3/662.5	9.3	30 K
H_2O:CO:O_2:N_2:CO_2=1:50:35:15:3	2138.1	5.6	2344.9	3.9	658.8/661.6(s)	6	10 K
H_2O:CO:O_2:N_2:CO_2=1:25:25:10:13	2140.3	7.6	2342.4	9.8	658.7/662.7(s)	9.8	10 K
H_2O:$C_{10}H_8$:CO=1:30:500	2137.7	7.9	-	-	-	-	10 K

plexes, but to those involving dangling OH bonds. The CO peak at 2150 cm^{-1} has not yet been observed in interstellar ices.

It should be possible to observe the 2150 cm^{-1} band in the interstellar medium. There are, however, several observational constraints, including overlap with the XCN band (2165 cm^{-1}) and gas-phase CO lines. High-resolution spectra are therefore required, and a detection could be made possible with ground-based observations. Future fitting procedures for astronomical CO observations must take into account the fact that polar and apolar CO band profiles may be difficult to distinguish, when CO_2 or O_2 are abundant in the apolar phase (see Sect. 4.3).

4.10. Effects of diffusion

CO, N_2 and O_2 sublime near 30 K under laboratory conditions (system pressure = 10^{-8} mbar). Pure CO_2 is less volatile and evaporates at a higher temperature of 80 K. During an increase in temperature, volatile components evaporate from the ice ma-

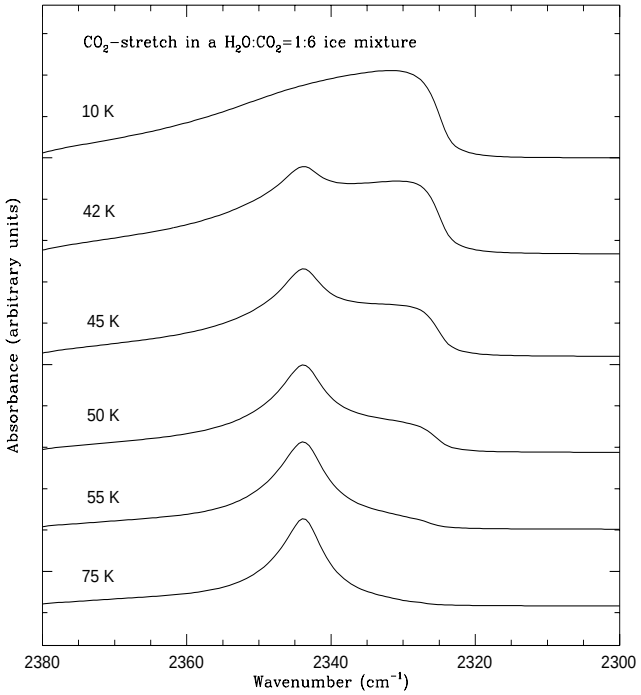

Fig. 10. Infrared absorption spectra of the stretching mode of solid CO_2 in a CO_2/H_2O=6:1 mixture during warm-up. Stepwise annealing revealed the two components which contribute to this large asymmetric CO_2 profile. The peak at 2344 cm^{-1} is due to pure CO_2, and the peak at 2328 cm^{-1} is likely due a second trapping site for CO_2. This site is destroyed when raising the temperature to 42 and 50 K. At 75 K, the band shows a profile similar to that of pure CO_2. The annealing process rearranges the matrix, and after warm-up the CO_2 and H_2O molecules exist within the matrix in a two-phase system.

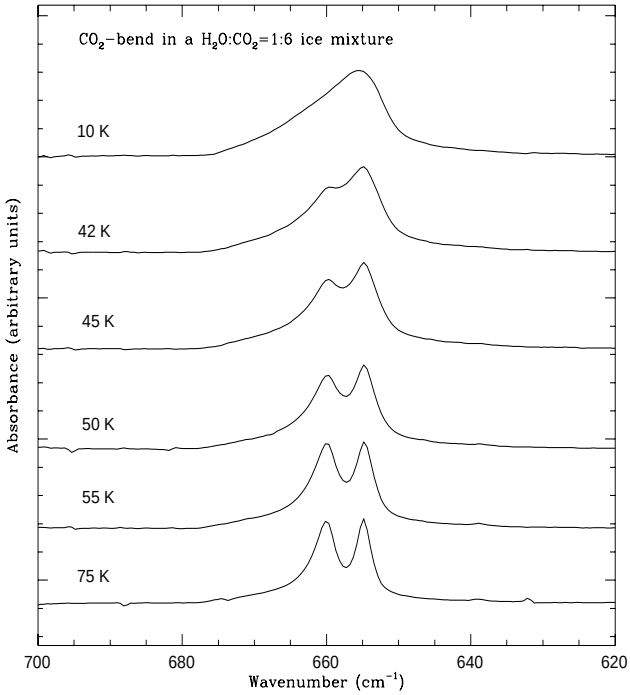

Fig. 11. Infrared absorption spectra of the bending mode of solid CO_2 in a CO_2/H_2O=6:1 mixture during warm-up. Stepwise annealing revealed the two components which contribute to this large asymmetric CO_2 profile. The strong asymmetric band may be due to aggregate formation, which is slowly converted into "pure" CO_2, showing the typical double-peaked structure.

trix and the matrix is rearranged. It is possible to monitor these changes through infrared spectroscopy. We have studied the spectral behavior of CO_2 in CO_2/H_2O mixtures, which is shown in Figs. 10 and 11. In Fig. 15, we show the changes in the CO band profile during warm-up to 30 K for several mixtures. Profiles with a large band width indicate strong interactions between the matrix constituents and therefore a fragile matrix. During the warm-up of such an easily-destroyed matrix, complexes and aggregates are broken and the ice components are separated: resulting in a strong decrease in band width and blueshifts, even for only a small increase in temperature.

4.11. Effects of UV photolysis

CO_2 is readily formed by UV photolysis of astrophysical ice analogs. We have studied the behavior of CO and CO_2 profiles in polar and apolar ice mixtures, and in "onion" structures during photolysis, see Fig. 16. An "onion" structure was simulated in the laboratory, by depositing an apolar mixture (containing CO, O_2, N_2, CO_2 and a small amount of H_2O) on top of an H_2O:CO=100:10 layer. All mixtures have a similar thickness of up to 0.15 μm (in order to ensure that they were optically thin to the UV flux). All samples were exposed to an equal amount of UV irradiation for 1 hr, corresponding to an interstellar radiation dose of $\sim 10^3$ years in the outer regions of interstellar clouds and to $\sim 10^8$ inside dense clouds (Gerakines et al. 1996). The parameters of CO and CO_2 profiles before and after UV irradiation are summarized in Table 8. Whereas the CO band is rather unaffected by the UV irradiation, the profiles of both the CO_2 stretching and bending modes are severely broadened. As a result, the two peaks of the bending mode are no longer well separated.

UV photolysis of polar H_2O/CO ice mixtures readily forms CO_2, with a broad stretching mode profile (15 cm^{-1}). The CO_2 band position falls at 2341 cm^{-1}, at lower frequencies as compared to that in apolar ices, with the exception of apolar mixtures which contain CO and CO_2 in similar amounts. The irradiation of pure CO (or CO mixed in with a small amount of water ice) creates a CO_2 band which is narrow and close to the position of gaseous CO_2 features. The narrow band width can be explained because CO_2 is only a minor species in the CO matrix and is therefore not exposed to strong interactions. The "blue" CO_2 band position of 2347 cm^{-1} is exceptional, however.

When CO_2 is formed by UV photolysis from polar, apolar or "onion" ices, the stretching mode remains rather consistent in both peak position (2341.1 - 2342.9 cm^{-1}) and in band width ($\sim$15 cm^{-1}). The bending mode is not so consistent. In the polar mixture, it is redshifted and very broad ($\sim$25 cm^{-1}). It is also

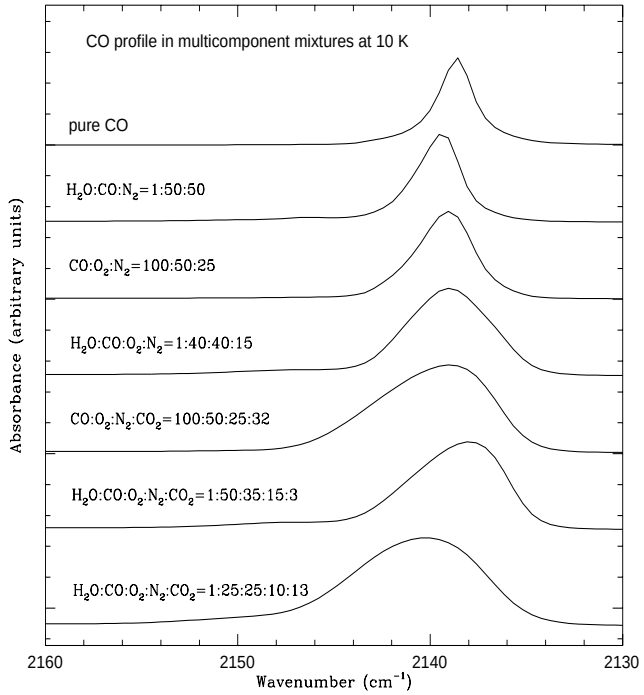

Fig. 12. Infrared absorption spectra of solid CO in multicomponent matrices. At equal abundances of CO and N_2, the CO band profile is blueshifted by $\sim 1\,\mathrm{cm}^{-1}$. The band width remains constant. N_2 has a crystalline structure similar to that of CO and seems rather inert. The presence of CO_2 and O_2 invokes a broadening of the CO band and a shift in its peak position, depending on the exact molecular composition of the ice mixture.

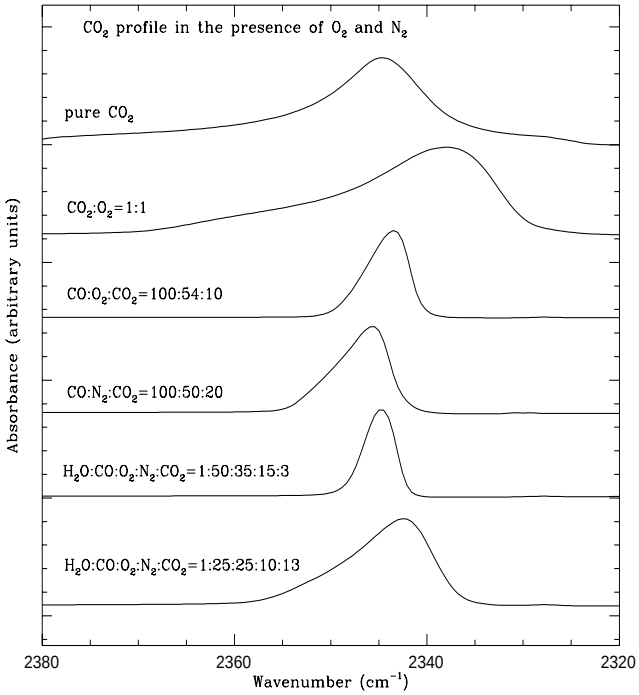

Fig. 13. Infrared absorption spectra of solid CO_2 in the presence of O_2 and N_2. A strong shift to lower frequencies and a large broadening are observed when the concentrations of O_2 and CO_2 are equal. Large concentrations of N_2 cause only a small blueshift of the CO_2 band and no additional broadening.

superimposed on the strong H_2O libration mode, which can drastically affect the accuracy of the measurement. However, the CO_2 bending mode as measured in the "onion" ices (also superimposed on the water libration mode) shows a band which is similar in band position and width to the apolar mixtures, see Table 8. It is interesting to note, that CO_2 deposited with a polar mixture and CO_2 produced by UV irradiation of a polar H_2O/CO mixture can spectroscopically not be distinguished (see Table 8 and 10).

We have furthermore determined the yield of CO_2 production from various matrices, see Table 9. The initial cross section for formation of CO_2, σ_F (in cm^2), may be derived from

$$\frac{\mathrm{d}N}{\mathrm{d}t} = \phi \cdot N_\mathrm{p} \cdot \sigma_\mathrm{F}, \quad (1)$$

where N is the CO_2 abundance, N_p the abundance of the parent CO and ϕ the flux of UV photons during the irradiation (see also Gerakines et al. 1996).

In Table 9, we compare the CO_2 yield of various ice mixtures, calculated per CO molecule and per photon. Nearly all of the CO was converted into CO_2 within the first 5 min. of irradiation in the H_2O:CO polar mixture. The spectrum remained constant after 1 hr of UV irradiation, reflecting that an equilibrium between CO_2 formation and destruction is reached after a very short timescale. Apolar mixtures, containing large concentrations of CO and O_2, and "onions" lead to an efficient CO_2 production (between 40 - 85 % relative that of polar mixtures). However, in apolar mixtures, a gradual increase of the CO_2 production rate was monitored during 1 hr of UV exposure. In such apolar mixtures (as well as in "onions"), competition with the production of O_3 reduces the amount of O atoms available to form CO_2. Irradiation of pure CO yields very little CO_2, see also Gerakines et al. (1996). The most efficient CO_2 production by far is achieved by irradiation of polar H_2O/CO mixtures (see Table 8).

5. Optical constants

5.1. Derivation of optical constants

The shape and peak position of strong absorption bands depend on the shape and size of the interstellar grain (see Sect. 6). For this correction accurate optical constants are needed. The optical constants were determined using a Kramers-Kronig analysis of the transmission spectra, following the method described by Hudgins et al. (1993). To summarize, the real part of the refractive index at all frequencies, $n(\nu)$, may be derived from the Kramers-Kronig dispersion relation:

$$n(\nu) = 1 + \frac{1}{2\pi^2} \int_0^\infty \frac{\alpha(\nu')}{(\nu'^2 - \nu^2)} d\nu', \quad (2)$$

Table 8. Band positions and widths (in cm^{-1}) of CO and CO_2 IR absorption features upon deposition (dep) and after 1 hr of UV irradiation (irr).

	^{12}CO stretch		$^{12}CO_2$ stretch		$^{12}CO_2$ bend	
Ice composition	Position cm^{-1}	FWHM cm^{-1}	Position cm^{-1}	FWHM cm^{-1}	Position cm^{-1}	FWHM cm^{-1}
pure CO_2 (dep)	-	-	2344.8	12.2	654.7/659.9	2.5/4.8
pure CO_2 (irr)	-	-	2343.2	15.6	655.0/659.9	11.7
pure CO (dep)	2138.6	2.5	-	-		- -
pure CO (irr)	2138.7	2.4	-	-		- -
H_2O:CO=100:20 (dep)	2137.3/2150	8/sh	-	-	-	-
H_2O:CO=100:20 (irr)	2139.8	14.1	2341.1	15.5	653.8	25.6
H_2O:CO:O_2:N_2:CO_2=1:50:35:15:3 (dep)	2138.6	5.4	2344.9	4.0	660.6	6.5
H_2O:CO:O_2:N_2:CO_2=1:50:35:15:3 (irr)	2141.1	8.4	2341.8	15.5	657.4	11.1
H_2O:CO=1:100 (dep)	2138.7	2.5	-	-	-	-
H_2O:CO=1:100 (irr)	2138.8	2.4	2347	3.7	658.0 /660.6	4.2
H_2O:CO:O_2=1:50:50 (dep)	2138.6	5.5	-	-	-	-
H_2O:CO:O_2=1:50:50 (irr)	2139.6	7.6	2342.9	15.5	657.3/660.8	10.5
onion: (dep)						
bottom – H_2O:CO=100:10						
top – H_2O:CO:O_2:N_2:CO_2=1:50:35:15:3	2138.1/2150	6.1	2344.7	3.8	-	-
onion: (irr)	2141.6	10	2341.1	15	656.6	15

where $\alpha(\nu)$ is the absorption coefficient given by

$$\alpha(\nu) = \frac{4\pi k(\nu)}{\lambda} = \frac{1}{h}\left[\tau(\nu) + \ln\left|\frac{\mathbf{t}_{01}\mathbf{t}_{12}/\mathbf{t}_{02}}{1+\mathbf{r}_{01}\mathbf{r}_{12}\exp(4i\pi h\mathbf{m}/\lambda)}\right|^2\right]. \quad (3)$$

Here, h is the thickness of the ice, $\tau(\nu)$ is its measured optical depth, $\mathbf{m}$ is the total *complex* refractive index ($\mathbf{m} = n + ik$), and $\mathbf{t}_{ij}$ & $\mathbf{r}_{ij}$ are the complex transmission and reflection coefficients at the $i-j$ boundary (where 0 = substrate, 1 = ice, 2 = vacuum).

In principle, we must carry out the integration in Eq. (2) over all frequencies. However, since electronic absorption bands (in the visible and UV parts of the spectrum) are well-separated in frequency space from the infrared, they contribute only a constant term to the integration in Eq. (2), which may then be approximated as:

$$n(\nu) \approx n_0 + \frac{1}{2\pi^2}\int_{IR}\frac{\alpha(\nu')}{(\nu'^2-\nu^2)}d\nu', \quad (4)$$

where n_0 is the real part of the ice's refractive index at high frequencies (as measured by previous authors; see Hudgins et al. 1993), and the integration is carried out over the infrared part of the spectrum.

Since $n(\nu)$ and $k(\nu)$ are not independent quantities, results must be obtained iteratively. To begin the iteration, we assume that at all frequencies $\mathbf{m}(\nu) = n_0$ (values of n_0 used here are identical to those used by Hudgins et al. 1993). Once both $n(\nu)$ and $k(\nu)$ have been calculated using Eqs. (3) & (4), they are used to create an "artificial" spectrum using Eq. (3) once more, and this is then compared to the original input spectrum. If the differences between the input and "artificial" spectra are too large, the iteration is continued with the new values of n and k as the starting point. In our case, iterations continued until the spectra agreed to within 0.1 % at each frequency point. Most spectra in the data set achieved convergence within 30 - 40 iterations, depending on the sharpness of the features and the smoothness of the baseline. The code used to calculate n and k was tested against a model for a Lorentz oscillator.

5.2. Baseline subtraction

To calculate accurate optical constants, the baseline of the laboratory spectra must be properly substracted. Ideally, the baseline of the observed transmission spectrum would have a sinusoidal pattern which is caused by interference of the waves reflected and transmitted at the vacuum-ice and ice-substrate interfaces. This can be corrected for in the derivation of the optical constants at a given ice thickness. However, various experimental effects may deform the baseline (see e.g., Hudgins et al. 1993). Hence the baseline must be removed by a polynomial fit. Near strong absorption modes, like the CO_2 stretching mode, the fitting region must be carefully chosen. The continuum at the blue and red sides of the absorption does not join up, due to a large difference in refractive index n (e.g. Fig. 19). This is intrinsic to the absorption band, and must not be artificially removed. We chose to subtract a global polynomial baseline (in general of order 4), avoiding fits close to the CO_2 stretching mode. Errors introduced by inaccuracies of the baseline determination were estimated to be maximally 2 %, or 5 % for some mixtures with very broad absorption bands (e.g. mixtures containing H_2O).

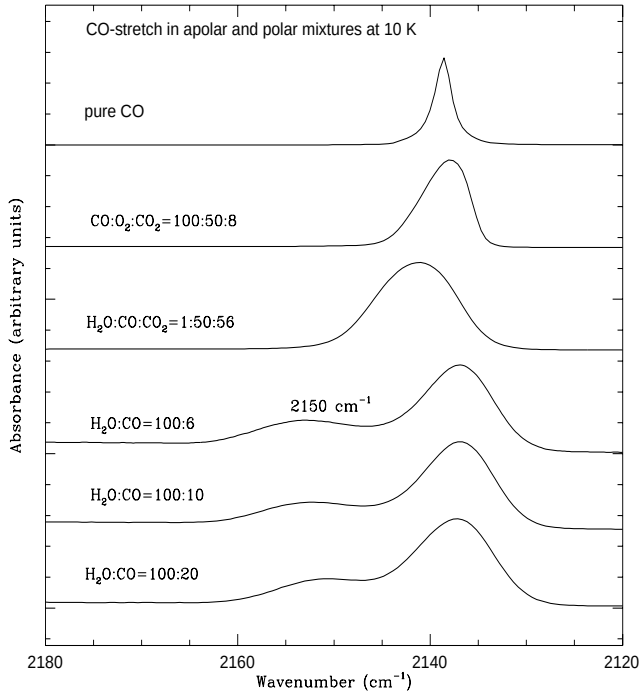

Fig. 14. Infrared absorption spectra of solid CO in polar and apolar mixtures. A large width is not only characteristic of polar mixtures, as previously assumed. In polar mixtures, an additional band at 2150 cm^{-1} is always observed. This band is likely due to a CO-H_2O complex.

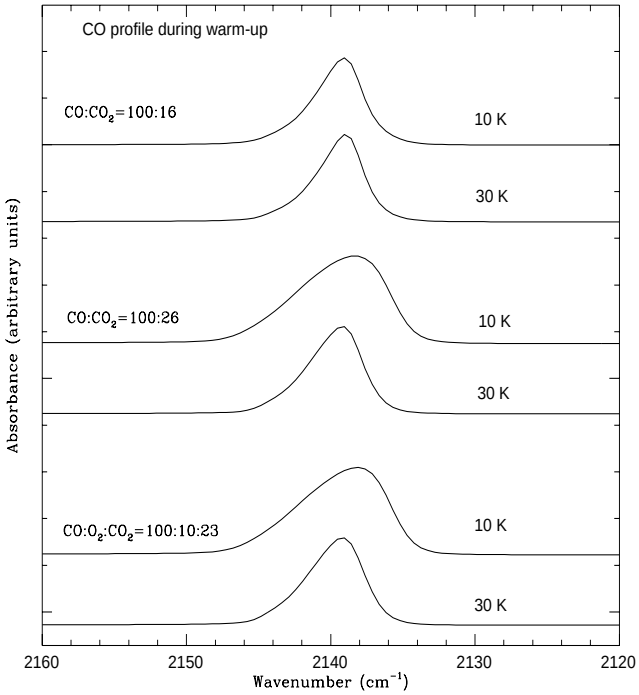

Fig. 15. Infrared absorption spectra of solid CO during annealing to 30 K. The profile of the CO:CO_2=100:16 mixture, which has a band width of 3.8 cm^{-1}, remains nearly unchanged when heated to 30 K, whereas the width of the CO band in the CO:CO_2=100:26 mixture is reduced from 7.4 cm^{-1} to 4.5 cm^{-1}. A 2.6 cm^{-1} reduction in width is also observed in the CO:O_2:CO_2=100:10:23 mixture during warm-up. Matrices with strong interacting components are easily destroyed during temperature rise.

Table 9. Yield of CO_2 production after 1 hr UV irradiation (in units of 10^{-19} cm^2 per CO molecule per photon).

Ice composition	σ_F 10^{-19} cm^2
pure CO	0.038
H_2O:CO=100:20	3.1
H_2O:CO:O_2:N_2:CO_2=1:50:35:15:3	2.7
H_2O:CO=1:100	0.097
H_2O:CO:O_2=1:50:50	1.2
onion:	
bottom – H_2O:CO=100:10	
top – H_2O:CO:O_2:N_2:CO_2=1:50:35:15:3	2.0

This uncertainty on absorbance scale is transferred directly to the optical constants (see Sect. 6.5).

6. Grain shape effects

6.1. Resonances

The interaction of electromagnetic radiation with an interstellar grain polarizes the grain, and the molecules within it experience applied and induced electric field components. This will change the shape and peak position of strong absorption bands. In the infrared, interstellar grains are smaller than the wavelength, and electrostatic theory applies. Also, extinction due to scattering can be neglected in this limit and a simple expression for the absorption cross section $C_{\rm abs}$ for ellipsoidal homogeneous particles can be derived (cf. Van de Hulst 1957, Bohren and Huffman 1983):

$$C_{\rm abs}/V = \frac{2\pi}{3\lambda} \sum_{i=1}^{3} \frac{2nk/L_i^2}{(1/L_i - 1 + n^2 - k^2)^2 + (2nk)^2} \quad (5)$$

where we have assumed that the grain resides in a vacuum. In this expression, V is the volume of the ellipsoid and n and k are the optical constants of the grain material, which are wavelength (λ) dependent. The geometry parameter L_i ($0 \leq L_i \leq 1$) characterizes the shape of the particle along each of the three major axes i. The summation over i assumes that the particles are randomly oriented in space. There will be a resonance in $C_{\rm abs}$ when $k^2 - n^2$ is comparable to $1/L_i - 1$. This implies that the profiles of strong absorption bands are very sensitive to the particle shape. Near strong molecular bands, n and k vary rapidly with wavelength and the peak position will depend on L_i, i.e. the particle shape. For a particular shape, the peak value of $C_{\rm abs}$ is then proportional to $1/nk$.

For spheres, $L_i = 1/3$ along each axis, and resonances occur at $k^2 - n^2 = 2$. Both weak and strong absorption bands will show a peak at large nk, near the frequency of the k peak. However, strong absorption bands will have a maximum $k^2 - n^2 > 2$, and a dominant second peak in $C_{\rm abs}$ arises at small nk towards

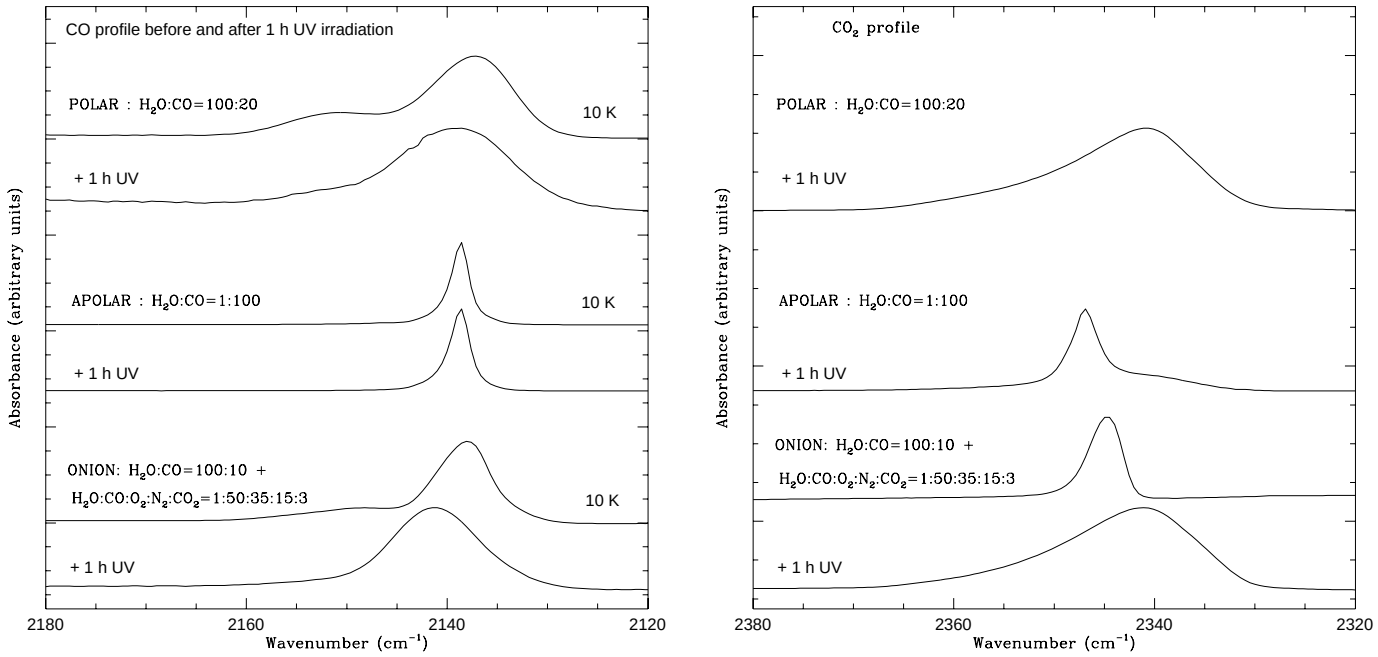

Fig. 16. (left) Infrared absorption spectra of solid CO in polar, apolar and "onion" type ices before and after 1 hr of UV irradiation. In the polar mixture, the shoulder of the CO band (centered near 2150 cm^{-1}) has disappeared after photolysis. The apolar CO band profile remains constant after photolysis, whereas the CO band broadens and shifts by 5 cm^{-1} to higher frequency in the "onion" ice. **(right)** Infrared absorption spectra of solid CO_2 produced by irradiation of polar, apolar, and "onion" type ices after 1 hr of UV irradiation. A broad CO_2 band is produced from the polar mixture, with a width of 15 cm^{-1}. The CO_2 band created by photolysis of apolar CO is narrow, since only a small amount of CO_2 is formed by this process. The CO_2 stretching mode formed from an "onion" type ice shows the same width and peak position than in a polar ice.

higher frequencies. For our optical constants of pure CO and CO_2 ices, this second resonance is respectively 6 and 8 times stronger than the resonance for high nk, and they have blended in one absorption peak. For spheroidal particles L_i will be the same along two axes, due to symmetry. For example, an oblate spheroid with a minor (i = 3) over major (i = 1, 2) axis ratio of 0.5 has L_3 = 0.54 and L_1 = L_2 = 0.23. In this case two dominant resonances will occur for strong bands, one at $k^2 - n^2$ = 1.6 along the minor axis and one at $k^2 - n^2$ = 3.3 along the major axes. Non-spheroidal ellipsoids will show three different absorption peaks, each resulting from an axis. Furthermore, for coated spherical particles, the core and mantle will be differently polarized and surface modes at each interface will induce two separate resonances. For example, a grain with a silicate core taking up 10 % of the total volume, will show resonances at $k^2 - n^2$=3.28 and 0.80 (using silicate optical constants at 4.4 μm; Laor and Draine 1993).

Thus, the profile of strong absorption bands depends strongly on the adopted dust model, and considerable deviations from the profile observed in the laboratory may occur. In this case, the laboratory ice transmission spectrum cannot be applied to astrophysical conditions, and grain shape calculations (and thus accurate optical constants) are required.

6.2. Calculations

We have calculated wavelength-dependent absorption cross sections for a number of different grain models in the small-particle limit. Standard formulae were applied for ice spheres, silicate spheres coated with an ice mantle (equal volume for core and mantle), and a distribution of ellipsoidally shaped particles with each shape equally probable ('CDE'; e.g. Van de Hulst 1957, Bohren and Huffman 1983). Additionally, a model for a distribution of coated spherical grain sizes was calculated. We assumed that the ice mantle thickness is independent of grain size, which follows from simple grain growth arguments (Draine 1985). Although our calculations are done in the small-particle limit, and C_{abs}/V is independent of grain size, the absorption profile is very sensitive to the ratio of grain core versus mantle volume (compare, for example, the pure ice spheres and the core-mantle grain in Figs. 18 and 20). Thus, in order to simulate the effect of a grain size distribution, we actually integrate over a distribution of core/mantle volume ratios, for a fixed mantle thickness and grain core size distribution. For this study, we used a mantle thickness of 0.01 μm and the interstellar grain size distribution derived by Mathis, Rumple and Nordsieck (1977; 'MRN'), i.e. a power law distribution of grain number density with grain radius of index -3.5 and cutoff radii of 0.005 and 0.3 μm. Note that for this MRN model C_{abs}/V has been normalized to the integrated total grain volume (cores+mantles).

We have done these calculations for the optical constants of our database of CO and CO_2 ices. For the pure ices, we compare the calculations using optical constants derived by different laboratory groups: Tielens et al. (1991; 'T91'), Hudgins et al. (1993; 'H93'), Trotta (1996; 'T96'), Trotta and Schmitt (1997),

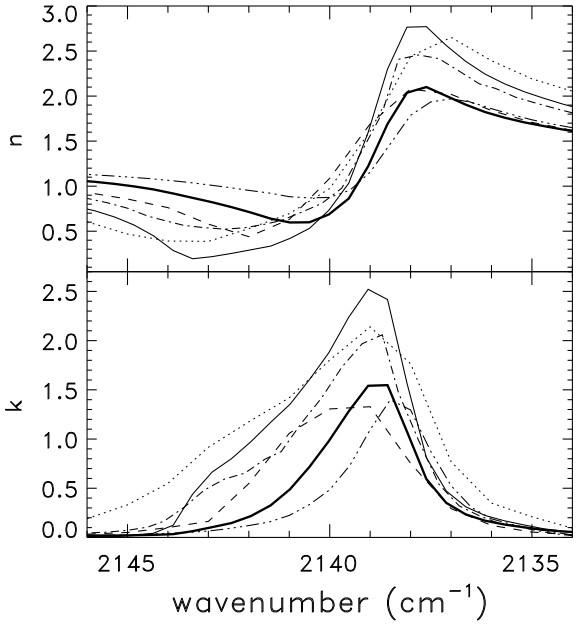

Fig. 17. The optical constants for the fundamental mode of pure CO ice, derived in different studies (see text for abbreviations): this work (thin solid line), B97 (dash), E97 (dash-dot), T96 (dash-triple dots), and T91 (dots). The thick solid line are the constants calculated from our transmission spectrum, assuming a two times larger sample thickness.

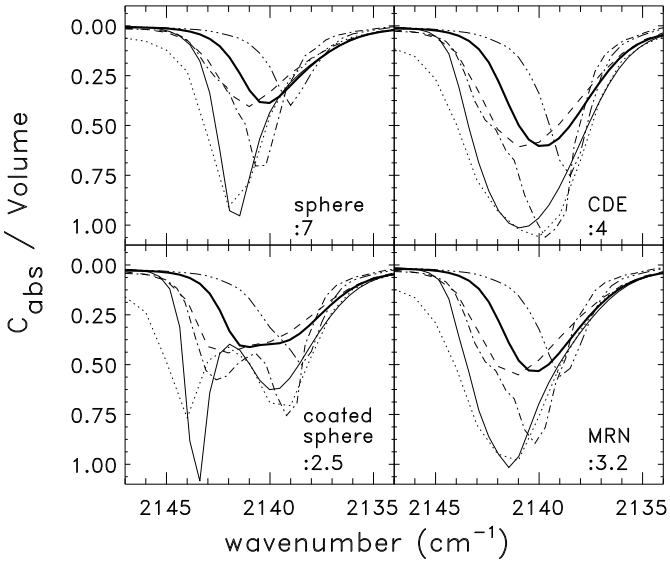

Fig. 18. Absorption cross sections for the pure solid CO fundamental mode for different dust models, using the optical constants shown in Fig. 17. Models in the small particle limit were calculated for pure ice spheres, silicate spheres with an ice mantle of equal volume, a continuous distribution of ellipsoids (CDE) and an MRN size distribution with 0.01 μm thick ice mantles and silicate cores. The cross sections have been scaled by the number given in the right-lower corner of each panel.

Elsila et al. (1997; 'E97') and preliminary data from Baratta et al. (1997; 'B97'). Furthermore, we test the effect of possible errors in the sample thickness, baseline subtraction and adopted electronic refractive index, n_0, on the optical constants and $C_{\rm abs}$ for the different grain models.

6.3. CO

The differences in the optical constants between the above mentioned studies of the solid CO fundamental absorption mode (Fig. 17) induce a large variation in sensitivity to the grain shape. The optical constants of T96 correspond to the weakest intrinsic strength, and are insensitive to the particle shape (Fig. 18). The peak and width of the profile are similar to the k-spectrum. Although the peak k value in the T96 data is the same as for B97, the latter shows a blueshift of 1.5 cm^{-1} after the calculations. Also a broadening of 1 - 1.5 cm^{-1} occurs for the B97 when applying size and shape distributions compared to pure ice spheres. This difference is caused by the presence of an extended blue wing in k for B97. The grain shape has the largest influence for T91 and our optical constants, inducing blueshifts up to 3 cm^{-1} compared to k, and large shifts and broadenings (2 - 4 cm^{-1}) between the different grain models. Both data sets have extensive wings in k towards the blue. The E97 sample has a peak k comparable to T91, but the blue wing is less pronounced. Consequently, the peak shifts and broadenings are reduced by almost a factor two for this sample. We emphasize that these shifts, broadenings and their uncertainties (comparing the different data sets) have the same magnitude as the matrix-induced variations discussed in this paper.

6.4. CO_2

Although the peak values of k are similar for CO and CO_2, the wavelength region with $k > n$ is broader and more pronounced for CO_2 (Fig. 19). This causes a much larger sensitivity of the absorption profile to the shape and size of the grains (Fig. 20). Like CO, large differences exist between the optical constants derived by different groups. Again, the T96 data have the lowest peak k value and are least sensitive to the grain shape calculations, However, in this case the effect is not negligible. Typically, peak shifts and broadenings of 5 cm^{-1} can occur. For the other datasets the effects are much larger, and in fact dominate over matrix-induced variations for CO_2-rich mixtures. The strongest broadening is observed for H93, i.e. up to 25 cm^{-1} for the CDE model compared to the laboratory spectrum. This broadening is only half for B97, and our data is in between these cases. For a pure CO_2 ice sphere, the width is comparable to the laboratory spectrum. However, whereas for the CDE model the peak is blueshifted by 6 cm^{-1}, the ice sphere shows a much larger blueshift ($\simeq$15 cm^{-1}) for both B97, H93 as well as our data. These peak shifts and broadenings reflect the presence of a deep minimum in n, and corresponding large k values for these datasets. For ices with a low CO_2 concentration ($< 10\%$), k is small compared to n and these grain shape effects are negligible.

The results for the bending mode of solid CO_2 are rather similar to the stretching mode. The H93 spectra are, like our data, very sensitive to grain shape effects in the 665 - 680 cm^{-1} region, where $k > n$. For a single coated sphere this gives rise to a third absorption peak, besides the two peaks corresponding to different trapping sites for pure CO_2 and heated CO_2 mixtures. However, for the shape and size distributions this third peak merges with the bluest of the trapping peaks. This results in a strongly asymmetric double-peaked profile, with a strong blue peak. Not surprisingly, the T96 sample does not show this effect, although the blue peak has slightly broadened.

6.5. Error propagation

We have investigated whether the remarkable differences between the CO and CO_2 optical constants derived in this paper and in T96 and B97 may be ascribed to an error in the assumed sample thickness. For CO, an increase of the thickness with a factor two results in a reasonable agreement in peak k and n values (Fig. 17). However, large differences remain in the strong absorption region long-ward of 2140 cm^{-1}, and thus in C_{abs} for the different grain models (Fig. 18). For the CO_2 stretch mode, a 2.7 times larger thickness would be needed to obtain a peak k value corresponding with T96 (Fig. 19). However, in this case the peak n value is too low, whereas for the bending mode a much larger sample thickness would be needed to obtain a good match. Not surprisingly, no good match is obtained for the corresponding cross section profiles (Fig. 20). These results indicate that an erroneous sample thickness (i.e. band strength and/or ice density) is not the main explanation for the observed discrepancies.

T96 and Trotta & Schmitt (1997) claim that the "classical" assumptions in the optical transfer (Sect. 5) used to derive n and k from the transmission spectra, may lead to an overestimation of k. This could be a reason for the discrepancy between the results of different groups. We refer to their work and B97 for a thorough discussion of their experimental methods.

Besides a possible error in the sample thickness, we investigated the propagation of uncertainties in a number of other parameters in the calculation of the optical constants and subsequent grain shape calculations. Eq. (5) shows that the peak value of C_{abs} is proportional to $1/nk$, and strong peaks require accurate optical constants.

First, we have calculated the optical constants using several values for the refractive index at high frequencies, n_0 for pure CO_2 ice. In this case, a 30 % spread was found in C_{abs} for the blue peak of the core-mantle sphere, when applying $n_0 = 1.22 \pm 0.02$. For the CDE and MRN models this uncertainty is reduced to 10 %. Also a systematic peak shift was observed (Fig. 21).

Second, for pure CO_2 a typical uncertainty of 1-2 % on absorbance scale is introduced by the baseline subtraction. This is transferred directly into k and amplified in the grain shape calculations. This effect is the strongest for the single core–mantle spheres, up to 6 % on C_{abs} scale, when using our experiment of pure CO_2. This is not very important compared to the uncertainties discussed above, although we stress that a careful baseline correction is required (see Sect. 5.2).

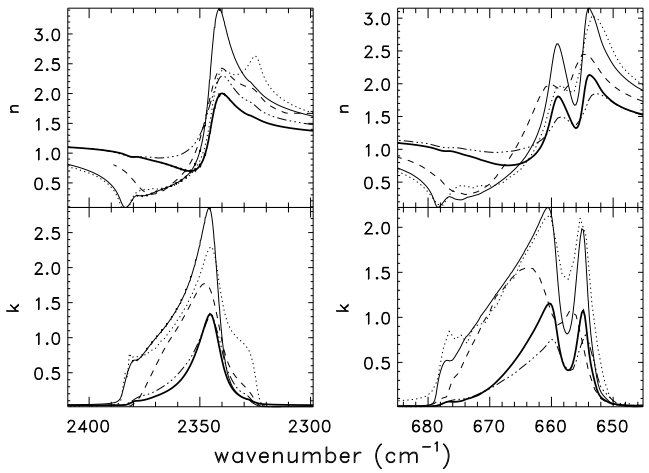

Fig. 19. The optical constants for the stretch (left) and bend (right) of pure CO_2 ice, derived in different studies: this work (thin solid line), B97 (dash), T96 (dash-triple dots), and H93 (dots). The thick solid line are the constants calculated from our transmission spectrum, assuming a 2.7 times larger sample thickness.

6.6. Summary

We have derived the optical constants of pure CO and CO_2 ice, applying the Kramers-Kronig analysis to the observed transmission spectra. Large discrepancies were found between the constants derived in 5 other studies. Our experiments were not designed to address the issue of optical constants directly and independently. Hence, no judgment can be made on this issue.

However, we do note that particle shape effects are important for strong transitions. They can lead to multiple peaks, peak shifts, and broadening of the absorption profile. The different optical constants were used to calculate these effects, and large differences were found. For CO, grain shape effects are important when the constants of E97, T91 and ours are used. The effects are smaller for B97, and negligible for T96. For CO_2, all investigated data sets are sensitive to the grain shape. Most sensitive are our data, H93 and B97. T96 is least sensitive, but still peak shifts and broadenings up to 5 cm^{-1} occur between the different dust models.

7. The astronomical cookbook

We have analysed the infrared spectra of 70 apolar mixtures containing CO, CO_2, O_2 and N_2. The basic rule is that O_2 and CO_2 invoke due to their electronic structure, strong interactions with each other and with CO. The molecule N_2 is rather inert. Therefore the strongest shifts and large broadening of CO and CO_2 band profiles occur in general when the components are equally abundant in the ice. A narrow CO or CO_2 band profile implies in general that no strong interactions occur between the ice components. For CO this is the case when pure or mixed

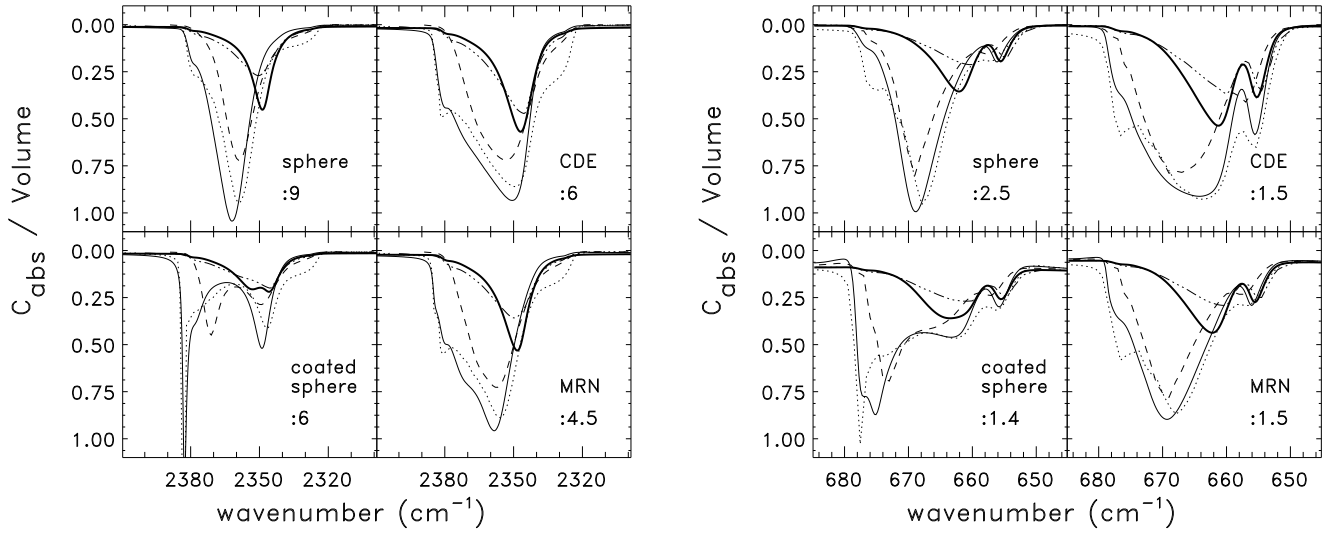

Fig. 20. Absorption cross sections for the pure solid CO_2 stretch (left) and bend (right) for different dust models, using the optical constants shown in Fig. 19. Models in the small particle limit were calculated for pure ice spheres, silicate spheres with an ice mantle of equal volume, a continuous distribution of ellipsoids (CDE) and an MRN size distribution with 0.01 μm thick ice mantles and silicate cores. The cross sections have been scaled by the number given in the right-lower corner of each panel.

with N_2 (also in large amounts) or small amounts of O_2 and CO_2 (up to a few %). In this case the FWHM does not exceed 3 cm^{-1}. In CO/O_2 mixtures a gradual increase in band width can be monitored with increasing O_2 concentration. A band width maximum of 5 cm^{-1} is reached when O_2 and CO are equally abundant (Sect. 4.2). In CO/CO_2 mixtures a dramatic change in band width occurs when CO_2 exceeds 21 % relative to CO and reaches a value of $\sim$ 10 cm^{-1}, when CO and CO_2 have equal abundance (see Sect. 4.3). This is also the largest band width of CO observed within 70 mixtures. The peak position of apolar CO shifts depending on the dilutant. Pure CO peaks at 2138.7 cm^{-1}. Large amounts of N_2 invoke blueshifts of $<$ 1 cm^{-1}. O_2 in large concentrations may induce a redshift of 1.3 cm^{-1}. Large concentration of CO_2 invoke blueshifts up to 2.5 cm^{-1}. In multicomponent mixtures the deviation of the CO band position from pure CO is not pronounced, because the various interactions between all ice components tend to cancel each other out. To summarize: a narrow apolar CO band excludes the presence of other molecules in the ice with the exception of N_2. A large band width confirms the presence of O_2 and CO_2, showing a red and blue shifted band respectively. When the band is broad (5 - 7 cm^{-1}) and only slightly shifted from the position of pure CO it indicates in general the presence of both molecules, CO_2 and O_2. However, some CO/CO_2 mixtures (e.g. $CO:CO_2$=100:26) also show similar spetroscopic characteristics. Polar CO (embedded in a water-rich mixture) displays in general a band width of 8 cm^{-1}, but appears at lower frequency (2137 cm^{-1}). Details are summarized in Table 10.

Pure CO_2 peaks at 2344.5 cm^{-1} and displays a broad feature (12 cm^{-1}) with pronounced wings. The bending mode of CO_2 is unique and shows a double structure (see Sect. 4.3). A narrow CO_2 band profile can only be observed when CO_2 is present in very low abundance within other components in the ice. Such a narrow band is also accompanied by a strong blueshift close to the gas phase position (2349 cm^{-1}). CO_2 interacts strongly with CO and O_2. In CO/CO_2 mixtures the band width increases from 3.1 cm^{-1} (4 % CO_2 relative to CO) to 19 cm^{-1} (when CO and CO_2 are in equal abundances). A large band width is also accompanied by a large redshift of the CO_2 band (5 cm^{-1} in the case of CO/CO_2=1:1). Extreme profiles with band shifts up to 15 cm^{-1} are observed in CO_2/H_2O mixtures when H_2O exceeds a few % in the ice. Such CO_2 bands are then unusually broad (up to 30 cm^{-1}) and easily distinguishable, see Fig. 9 and 10. A wide CO_2 band ($>$ 15 cm^{-1}) which is strongly redshifted does indicate the presence of abundant O_2. The CO_2 band blue-shifts in the presence of N_2 but does not show broadening.

The spectroscopic properties of multicomponent mixtures are the result of many different interactions of the various molecules present. In order to derive reliable abundances of infrared inactive molecules, the profiles of CO and CO_2 bands as well as their isotopes have to be carefully deconvolved. Polar CO_2 peaks at 2341 cm^{-1} and has a band width of 15 cm^{-1}. The CO_2 bending mode is then superimposed on the H_2O libration mode and polar CO_2 can be well recognized. The details are summarized in Table 10.

Warm-up leads to changes in the matrix configuration. Volatile molecules may evaporate, and species (such as H_2O), which are distributed within the matrix tend to polymerize (Ehrenfreund et al. 1996b). In general, bands in multicomponent mixtures sharpen and shift after temperature rise and are in some cases hard to distinguish from pure ices, see Sect. 4.5. Additional changes of the profiles of the CO and CO_2 bands can be induced depending on the grain shape, summarized in Sect. 6. The effects are largest for pure CO_2. For example, a blue-shift of

$\sim$13 cm^{-1} and a broadening of $\sim$20 cm^{-1} occur for an MRN grain size distribution with 0.01 μm thick ice mantles. However, at present the optical constants for both CO and CO_2 are uncertain. Future work on the optical constants will indicate us the role of particle shape calculations in order to infer correct band profiles. In any case, grain shape effects are not important at low CO ($< 30\%$) and CO_2 ($< 10\%$) concentrations.

8. Discussion

For several years, astronomical observations have proposed the existence of apolar ices. These ices may exist as an additional layer on top of polar ice layers in the form of an "onion" structure. Apolar ices may also exist as an entirely different grain population residing in the same line-of-sight. Apolar grain mantle components reflect the low accretion rates of atomic H. Under these conditions, grain mantles will be dominated by CO, O_2, N_2 or by CO_2. Whereas CO, N_2, and O_2 evaporate around 20 K under astrophysical conditions, CO_2 is somewhat less volatile and would survive closer to the star (up to T=45 K).

First ISO results show that in many lines-of-sight CO_2 ice is more abundant than CO. ISO detected also gaseous CO_2 in very low abundance, with a few % compared to solid CO_2 (van Dishoeck et al. 1996). CO_2 has been detected as a major volatile in the coma of comet Hale- Bopp with ISO at 4.6 and 2.9 AU from the Sun (Crovisier et al. 1996, 1997). The implications of recent ISO observations of interstellar ices, such as CO_2, for comets are discussed in Ehrenfreund et al. (1997a). There are not yet indications for the presence of the infrared inactive molecules O_2 and N_2. Recent results indicate large amounts of atomic oxygen and N_2 in the gas phase which may account for most of the oxygen and nitrogen currently missing in the interstellar budget. However, a certain percentage of O_2 and N_2 may still be included in the solid phase (Ehrenfreund & van Dishoeck 1997). Our laboratory results show, that fingerprints of O_2 and N_2 may be traced in the profiles of CO and CO_2 (see Sect. 7).

From the first ISO spectra, which show the unique double-peaked structure of the CO_2 bending mode at 15 μm, we can conclude that in addition to polar CO_2, a grain mantle layer of pure or annealed "apolar" CO_2 is present in the lines-of-sight towards several molecular clouds (representing different temperatures and evolutionary states). Our laboratory results indicate that the interstellar signature of apolar CO_2, (currently observed with ISO) resembles that of annealed or irradiated CO_2, rather than pure CO_2 at 10 K. The numerous narrow apolar CO band profiles observed by ground-based observations also prove that most of the apolar CO_2 is not mixed in the apolar phase together with CO. Our laboratory results show that the presence of CO_2 in an abundance of 20 % compared to CO in the ice broadens the CO band already to more than 5 cm^{-1}. This is currently not observed: the band width of apolar CO falls well below this value (Tielens et al. 1991, Chiar et al. 1994). However, CO_2 is apparently more abundant in the polar phase and preliminary estimates for polar:apolar CO_2 ratios range from 1.1 - 1.8 (Gerakines et al. 1997).

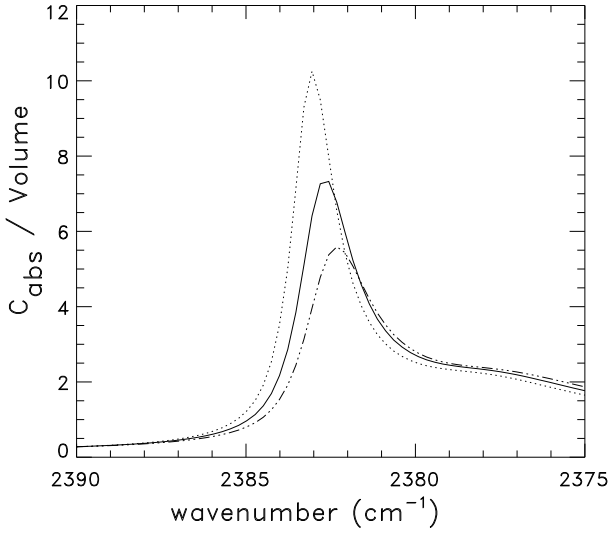

Fig. 21. The peak value and position of the blue absorption peak for the spherical grain, coated with pure CO_2 is very sensitive to the accuracy of the optical constants. The solid line shows the cross section, assuming n_0 = 1.22, the dotted line is for n_0 = 1.20 and the dash-dot line for n_0 = 1.24.

The existence and distribution of ice types have strong implications for interstellar chemistry and allow to reconstruct the line-of-sight conditions. In comparison with laboratory data we can envisage a consistent scenario where CO_2, formed by UV irradiation from H_2O/CO ices, resides in the polar phase and segregates out of this polar phase in temperature zones > 20 K, where volatile molecules such as CO, O_2, and N_2 are already evaporated. In those regions CO_2 or annealed CO_2/H_2O grain mantle layers may remain on top of grain mantle dominated by polar H_2O ice.

In Sect. 4.9, we have determined the CO_2 production yield. A main route of CO_2 formation will be the UV photolysis of H_2O/CO ices near protostars. Due to the extreme efficiency of this reaction (see e.g., Table 9), CO_2 may also be formed in this way inside dense regions which are far from protostars. Cosmic-ray excitation of H_2 molecules will provide a source of UV photons in embedded clouds, with an expected flux of 10^3 photons per cm^2 per second (Sternberg et al. 1987). However, Tielens & Whittet (1997) argue that long accretion timescales in space may allow oxidation reactions, forming CO_2 from CO an O on grains. Future observations along lines of sight with low amounts of grain processing and laboratory experiments of reaction kinetics will reveal the conditions which promote CO_2 formation.

First ISO results show that CO_2 must be introduced as an important molecule in the chemical networks of interstellar gas-phase chemistry. This will open new pathways and force us to also consider the reaction products of CO_2, such as CO_3, C_3O, O_3, and many others.

Table 10. Variation in the CO band profile

Ice type	Band position range cm^{-1}	Band width range cm^{-1}	Matrix effects
pure CO	2138.7	2.2	-
mixed with N_2 (1-50 %)	2138.8-2139.4	up to 3	only very small blueshifts, no broadening
mixed with N_2 and O_2	2139.1	3.3 - 5	increasing concentration of O_2 broadens the band, position stable
mixed with O_2 (20-50 %)	2137.4-2138.8	3.3 - 5.5	small redshifts, broadening of 2 cm^{-1} when CO:O_2=1:1
mixed with CO_2 (4-50 %)	2138.4-2141.3	2.5 - 9.6	increasing concentration of CO_2 leads to blueshifts, broadening of 7 cm^{-1} when CO:CO_2=1:1!
mixed with O_2 and CO_2	2137.6-2139.6	4.3 - 7.2	increasing concentration of CO_2 broadens the band, band position is stable, red-and blueshifts cancel out
mixed with multicomponents	2137.7-2140.3	4.0 - 8.0	band width is increasing when CO_2 and O_2 are abundant relative to CO, band position varies strongly
polar CO ice	2137/2150	8 (plus shoulder)	-

Table 11. Variations in the CO_2 stretching mode profile

Ice type	Band position range cm^{-1}	Band width range cm^{-1}	Matrix effects
pure CO_2	2344.8	12.1	-
mixed with O_2	2338.2	16.5	large redshifts and broadening when CO_2:O_2=1:1
mixed within CO (4-50 %)	2339.7-2346.7	3.1 - 19	redshifts and broadening with increasing CO_2 concentration
mixed within CO and O_2 (4-50 %)	2342.4-2346.3	4.9 - 7.3	redshifts and broadening with increasing CO_2 concentration
mixed with H_2O ice	2330-2332!	28 - 31	asymmetric profile with extreme redshift and strong broadening, when $H_2O > 10$ %
mixed with multicomponents	2342.0 -2346	4.0 - 10.0	band position and width are changing depending on the other molecules present
polar CO_2 ice	2341	15	-

Table 12. Variations in the CO_2 bending mode profile

Ice type	Band position range cm^{-1}	Band width range cm^{-1}	Matrix effects
pure CO_2	654.7/659.9	2.6/4.7	double peak
mixed with O_2	658	12	large redshifts and broadening
mixed within CO (4-50 %)	656.6 - 659.4	2.5 - 11	broadening with increasing CO_2 concentration CO_2 bend reaches 11 cm^{-1} when CO:CO_2=1:1
mixed within CO and O_2 (4-50 %)	658-659	5 - 8	up to 3 subpeaks and shoulders can be observed depending on the mixture
mixed with H_2O ice	655 !	11-12	asymmetric profile with extreme redshift and strong broadening
mixed with multicomponents	658-659	6.0 - 10.0	band position and width are changing depending on other constituents different subpeaks can be seen around 661 cm^{-1}
polar CO_2 ice	653	25	-

9. Conclusions

This paper summarizes the spectroscopic properties of a database of apolar ice analogs and discusses their astrophysical implications. We remind that this database can be found on the www: http://www.strw.leidenuniv.nl/∼ehrenfreund/isodb, and includes a help page for explanations. Using this database, observers can try to fit their measured profiles themselves, and assess the influence of any particle shape using the optical constants. It has been shown that the optical constants obtained by five different groups do differ strongly. As long as no consensus is reached on this subject, particle shape calculations have to be used with caution. However it is evident that such particle shape calculations are important, at least for CO_2 features. Our database is therefore dynamical and regularly updated.

Current ISO observations show a constant CO_2 profile in various lines-of-sight indicating the presence of CO_2-rich ices, which can be explained by the wings in the CO_2 stretching mode and the double-peak structure in the CO_2 bending mode.

An even larger fraction of CO_2 is observed in the polar phase towards the same targets. These two components likely indicate the formation of CO_2 from UV photolysis of H_2O/CO ices close to the protostar and a grain mantle component formed in a temperature zone > 20 K when CO_2 is segregating out of the polar phase. In comparison with astronomical observations the laboratory data on the stretching and bending mode of $^{12}CO_2$ and the $^{13}CO_2$ isotope provide a powerful diagnostic in order to determine the exact ice composition of interstellar grains. The presented database will enable to derive more exact ratios of polar/versus apolar ices using χ^2 calculation on incoming ISO data (Gerakines et al. 1997). With additional observations of the CO band (ground based and ISO) we can determine existing ice-types, ice structure (amorphous or crystalline) and temperature and irradiation conditions in the line-of-sight towards protostars. Column densities can be determined for CO and CO_2 ices as well as upper limits on the presence of solid O_2 and N_2 ice. To reconstruct the different cloud components and line-of sight conditions towards embedded protostars will provide important constraints on the evolution of molecular clouds.

Acknowledgements. We want to thank G. Baratta, M. Palumbo, G. Strazulla from the University of Catania and B. Schmitt and E. Trotta from the Laboratoire de Glaciologie Grenoble, for the permission to integrate their unpublished optical constants for CO and CO_2 ice in our paper, in order to allow a global overview on this still debated topic. PE wishes to thank W. Schutte for many fruitful discussions and C. Dominik for computer support. PAG wishes to thank F. Rouleau for his help in understanding the optical constants calculations. The laboratory work was supported by the European Community grant ER-BCHBICT940939. PAG is supported by NASA grant NAGW-4039. PE is a recipient of an APART fellowship of the Austrian Academy of Sciences.

References

Baratta et al., 1997 (in preparation; B97)
Barnes A.J., Szczepaniak K., Orville-Thomas W.J., 1980, J. Mol. Struc. 59, 39
Bohren C. F., Huffman D.R., 1983, Absorption and Scattering of Light by Small Particles. John Wiley & Sons, New York, Ch. 5
Boogert A. et al., 1996, A&A 315, L377
Chiar J. E., Adamson A. J., Kerr T. H., Whittet D. C. B., 1994, ApJ 426, 240
Chiar J. E., Adamson A. J., Kerr T. H., Whittet D. C. B., 1995, ApJ 455, 234
Crovisier J., et al., 1996, A&A 315, L 361
Crovisier J., et al., 1997, Science 275, 1904
d'Hendecourt L. B., Allamandola L. J., Greenberg J. M., 1985, A&A 152, 130
d'Hendecourt L. B., Allamandola L. J., Grim R., Greenberg J. M., 1986, A&A 158, 119
d'Hendecourt L. B., Jourdain de Muizon M., 1989, A&A 223, L5
d'Hendecourt L.B., Ehrenfreund P., 1996, Proceedings: "The Role of Dust in the Formation of Stars", ESO, Munich, September 1995, 301
d'Hendecourt L.B., et al., 1996, A&A 315, L365
de Graauw Th. et al. 1996, A&A 315, L345
Dorschner J., Henning T., 1995, A&AR 6, 271
Draine, B.T. 1985, in Protostars and Planets II, ed. D. Black & M. Mathews (Tucson: Univ. of Arizona Press), 621
Ehrenfreund P., Breukers R., d'Hendecourt L., Greenberg J. M., 1992, A&A 260, 431
Ehrenfreund P. et al. 1996a, A&A 315, L341
Ehrenfreund P., Gerakines P.A., Schutte W.A., van Hemert M., E.F. van Dishoeck, 1996b, A&A 312, 263
Ehrenfreund P., van Dishoeck E.F., 1997, Advances in Space Research, in press
Ehrenfreund P., d'Hendecourt L., Dartois E., Jourdain de Muizon M., Breitfellner M., Puget J.L., Habing H.J., 1997, Icarus, in press
Ehrenfreund P. et al. 1997b, in preparation for J. Chem. Phys.
Elsila J., Allamandola L.J., Sandford S.A., 1997, ApJ 479, 818 (E97)
Gerakines P.A., Schutte W. A., Greenberg J. M., van Dishoeck E. F., 1995, A&A, 296, 810
Gerakines P.A., Schutte W. A., Ehrenfreund P., 1996, A&A 312, 289
Gerakines P.A. et al. 1997, in preparation for ApJ
Grim R.J.A., Baas F., Geballe T.R., Greenberg J.M., Schutte W., 1991, A&A 243, 473
Hagen W., Tielens A. G. G. M., 1981, J. Chem. Phys. 75, 4198
Hudgins D. M., Sandford S. A., Allamandola L.J., Tielens A.G.G.M, 1993, ApJS 86, 713 (H93)
Jenniskens P., Blake D.F., Wilson M.A., Pohorille A., 1995, ApJ 455, 389
Laor, A., & Draine, B.T. 1993, ApJ 402,441
Mathis J. S., Rumpl W., Nordsieck K. H., 1977, ApJ 217, 425
Palumbo M. E., Strazulla G., 1993, A&A 269, 568
Sandford S.A., Allamandola L.J., Tielens A.G.G.M., Valero L.J. 1988, ApJ 329, 498
Sandford S. A., Allamandola L. J., 1990, ApJ 355, 357
Schmitt B., Greenberg J.M., Grim, P., 1989, ApJ 340, 33
Schmitt B., 1994, in: Molecules and grains in space, ed. Nenner I. AIP press, New York, 735
Skinner C.J., Tielens A.G.G.M., Barlow M.J., Justtanont K., 1992, ApJ 399, L79
Stacey G.J. et al., 1993, ApJ 404, 219
Sternberg A., Dalgarno A., Lepp S.,1987, ApJ 320, 676
Tielens A. G. G. M., Tokunaga A. T., Geballe T. R., Baas F., 1991, ApJ 381, 181 (T91)
Tielens A. G. G. M., Whittet, D.B.C., 1997, Proceedings: Molecules in Astrophysics: Probes and Processes, ed. E.F. van Dishoeck, Kluwer Dortdrecht, 45
Trotta F., 1996, Thesis, LGGE-CNRS, Université Joseph Fourier, Grenoble, France (T96)
Trotta F., Schmitt, B., 1997, Applied Spectroscopy (in preparation)
van Dishoeck E.F., et al., 1996, A&A 315, L 349
Van de Hulst H.C., 1957, Light Scattering by Small Particles. John Wiley & Sons, New York, Ch. 6
Weber P., Greenberg J. M., 1985, Nature 316, 403
Whittet D.C.B., Walker H.J., 1991, MNRAS 252, 63
Whittet D. C. B., Duley W. W., 1991, A&AR 2, 167
Whittet D. C. B., 1993 in: Dust and chemistry in astronomy, eds. Millar T. J., Williams D. A., IOP Publ. Ltd. Bristol, 1
Whittet D.C.B. et al., 1996, A&A 315, L357
Willner S. P., Gillet F. C., Herter T. L., et al., 1982, ApJ 253, 174

This article was processed by the author using Springer-Verlag LaTeX A&A style file *L-AA* version 3.